Bioorganic Chemistry 116 (2021) 105336

Contents lists available at ScienceDirect

Bioorganic Chemistry

journal homepage: www.elsevier.com/locate/bioorg

Design and synthesis of novel furan, furo[2,3-*d*]pyrimidine and furo[3,2-*e*][1,2,4]triazolo[1,5-*c*]pyrimidine derivatives as potential VEGFR-2 inhibitors

Menna M.A. Abd El-Mageed, Amal A.M. Eissa, Awatef El-Said Farag, Essam Eldin A. Osman *

Department of Pharmaceutical Chemistry, Faculty of Pharmacy, Cairo University, Kasr Alaini Street, 11562 Cairo, Egypt

ARTICLE INFO

Keyword:
Furan
Furo[2,3-*d*]pyrimidine
Furo[3,2-*e*][1,2,4]triazolo[1,5-*c*]pyrimidine
VEGFR-2
Angiogenesis
HUVECs

ABSTRACT

Novel furan **6a-c**, furo[2,3-*d*]pyrimidine **7a-f**, **9**, **10a-f**, **12a,b**, **14a-d** and furo[3,2-*e*][1,2,4]triazolo[1,5-*c*]pyrimidine **8a-f** derivatives were designed based on their structural similarity to a previously described oxazole VEGFR-2 back pocket binding fragment. The designed compounds were synthesized and screened for their *in vitro* VEGFR-2 inhibitory activity where they exhibited good to moderate nanomolar inhibition with improved ligand efficiencies. **8b** and **10c** (IC_{50} = 38.72 ± 1.7 and 41.40 ± 1.8 nM, respectively) were equipotent to sorafenib and **6a, 6c**, **7f, 8a, 8c, 10b, 10f, 12b**, **14c** and **14d** showed good activity (IC_{50} = 43.31–98.31 nM). The furotriazolopyrimidines **8a-c** and furopyrimidine derivative **10c** were further evaluated for their *in vitro* antiproliferative activity against human umbilical vein endothelial cells (HUVECs) where **8b** showed higher potency than sorafenib and resulted in cell cycle arrest at G2/M phase whereas **8c** revealed good antiproliferative activity with cell cycle arrest at G1 phase. Moreover, **8a-c** and **10c** showed significant inhibitory effects on the invasion and migration of HUVECs. Molecular docking study was conducted to gain insight about the potential binding mode. The furo[3,2-*e*][1,2,4]triazolo[1,5-*c*]pyrimidine derivatives **8b** and **8c** represent interesting starting point for antiangiogenic compounds based on their activity and favorable drug likeness profiles.

1. Introduction

Cancer is a global chief public health problem and is the second prominent cause of death globally according to estimates of World Health Organization (WHO)[1–4].The ability of cancer cells to spread to other organs, metastasis, increases its rate of morbidity and mortality [5,6]. Neovascularization, angiogenesis and lymphangiogenesis, is needed for metastasis[6], as well as tumor growth and progression. Without adequate blood supply, tumor cells cannot grow more than 2 mm^3 and become necrotic[5,6]. Consequently, angiogenesis is considered one of potential targets in cancer chemotherapeutic agents design [6–8]. Angiogenesis is believed to be modulated *via* activator and inhibitor components where both up-regulation of activators and down regulation of inhibitors play crucial roles[5,9]. Stimulatory effect of different angiogenic factors initiates endothelial cells for new capillary vessels formation[10]. This takes place through multiple steps including basement membrane dissolution, migration, and proliferation of endothelial cells[10]. Then, formation of new capillary vessels and survival of the newly formed blood vessels[10]. Vascular endothelial growth factors (VEGFs) and their tyrosine kinase receptors (VEGFRs) play crucial role in neovascularization[8]. VEGF-A is an essential VEGF family member that exerts its effect through binding to VEGFRs to stimulate autophosphorylation of certain tyrosine residues, resulting in downstream signaling essential for angiogenesis[10]. VEGFR-2 (KDR/Flk-1) is considered the most important subtype of VEGFRs and the essential mediator of angiogenesis[11]. VEGF/VEGFR pathway is involved in progression of many types of cancers as breast, colon, gastric and lung through migration, metastasis and angiogenesis activation[12]. Therefore, blocking VEGF-A and/or VEGFR-2 appears critical for inhibiting angiogenesis[13]. The monoclonal antibody bevacizumab (Avastin®), the first FDA approved angiogenesis inhibitor agent, inhibits VEGF-A [14]. Alternatively, several heterocyclic compounds inhibit angiogenesis through VEGFR-2 blockage. Small molecule inhibitors of VEGFR include oxindole derivatives as sunitinib **I** (IC_{50} = 10 nM)[15] and SU5416 **II** (IC_{50} = 1.04 ± 0.53 μM)[16], pyridine derivatives as sorafenib **III** (IC_{50} = 90 nM) [17,18] and apatinib **IV** (IC_{50} = 1 nM)[19], quinoline derivatives as tivonazib **V** (IC_{50} = 0.16 nM)[20], quinazoline derivatives as vanditanib **VI** (IC_{50} = 40 nM) [21,22], oxazole derivatives as **VII** (IC_{50} = 50 μM)[23], pyrazolopyrimidine derivatives **VIII** (IC_{50} = 37 nM)[24,25], and furo[2,3-*d*]pyrimidine derivatives as **IX** (IC_{50} = 122

* Corresponding author.

https://doi.org/10.1016/j.bioorg.2021.105336
Received 14 June 2021; Received in revised form 2 September 2021; Accepted 4 September 2021
Available online 8 September 2021
0045-2068/© 2021 Elsevier Inc. All rights reserved.

nM)[26], (Fig. 1). As with other kinase inhibitors, VEGFR-2 inhibitors can be classified into three major types. Type I inhibitors bind to the conservative ATP active site through H-bond formation with the hinge region[27]. Type I inhibitors, as sunitinib **I,** mostly bind to the active (DFG-in) conformation of VEGFR-2[27,28]. On the other hand, type II inhibitors bind to the inactive (DFG-out) conformation exploiting an allosteric binding site adjacent to the ATP binding site that is formed upon conformational changes in the phenylalanine residue of the DFG motif [27,28]. Type II inhibitors exemplified by sorafenib **III** can form H-bond and hydrophobic interactions with the allosteric site in addition to H-bonds formed with hinge region[29]. Since the allosteric pocket is much less conserved compared to the ATP binding pocket, this makes type II inhibitors more selective and more advantageous than type I inhibitors [27,29]. Type III or allosteric inhibitors bind exclusively to the less conserved allosteric pocket which makes this type of inhibitors highly selective[28,29]. The relatively low molecular weight oxazole fragment **VII** is considered a type III inhibitor[23].

VII is a VEGFR-2 kinase back-pocket binder that has been identified through a fragment-based drug design (FBDD) campaign. This fragment was considered a kinase family-specific fragment that preferentially inhibits the non-phosphorylated VEGFR-2 constituting a starting point for further optimization[23]. While generating a fragment that engages in binding with the hinge- region is straightforward; the design of a back pocket-binding fragment is a more challenging and tends to be more kinase family-specific. The strategy is known as "back-to-front" and involves starting with a putative back pocket-binding fragment and subsequently elaborating toward the hinge. The solved co-crystal structure of **VII** in complex with VEGFR-2 (PDB: **3VHK**) confirmed the occupancy of VEGFR-2 back pocket[23]. Interestingly, the phenyl ring of **VII** slightly overlap with the adenine binding site. This phenyl ring is flanked by Phe1047 in the DFG loop, where it forms an edge to face π-π interaction. Additionally, the nitrogen of the oxazole ring in **VII** is forming H-bond with the backbone NH of Asp1046 whereas its 3-hydroxylmethyl-aryl moiety is deeply positioned at the hydrophobic part of the back pocket, surrounded by Ile888, Leu889, Ile892, Val898, Leu1019, His1026, and Ile1044. (Fig. 2). The low binding affinity of this fragment (IC_{50} = 50 μM) seems reasonable based on its ligand efficiency (LE) and having no more than one violation of the "rule of three" (molecular mass ≤ 300, cLog P ≤ 3, H-bond donors ≤ 3, and H-bond acceptors ≤ 3) that classically describes fragment-like molecules. It was suggested to represent an interesting starting point for a "back-to-front" growth strategy where the molecular structure may be extended to bind Cys919 at the hinge region.

The present investigation describes the design and synthesis of novel furan, furo[2,3-*d*]pyrimidine and furo[3,2-*e*][1,2,4]triazolo[1,5-*c*]pyrimidine derivatives that could mimic the binding of **VII** at the hydrophobic back pocket of VEGFR-2 by maintaining its essential pharmacophoric features. Contrarily, the designed molecules are generally more rigid compared to **VII**. The highly rigid 2,8-diarylfuro[3,2-*e*][1,2,4]triazolo[1,5-*c*]pyrimidine derivatives showed perfect alignment to the 3D bioactive conformer of **VII**, (Fig. 4). The retrosynthetic precursors, *N*-(4-imino-6-arylfuro[2,3-*d*]pyrimidin-3(4*H*)-yl) acidamide and *N*′-(((3-cyano-5-(4-methoxyphenyl)furan-2-yl)imino) methyl)-acidhydrazide derivatives were included as less rigid analogues where their imine or cyano moieties may serve as hydrogen bond acceptors to the backbone NH of Asp1046. Alternatively, the imino group may serve as hydrogen bond donor to the backbone oxygen of Asp1046 or its carboxylic side chain. A fourth series of 3-(arylideneamino)-6-phenylfuro[2,3-*d*]pyrimidin-4(3*H*)-imine derivatives was designed to transform the partially rigid hydrazide into a more rigid analogue. Structure extension was considered through the introduction of variable H-bond acceptor and/or donor functional groups into the arylidene

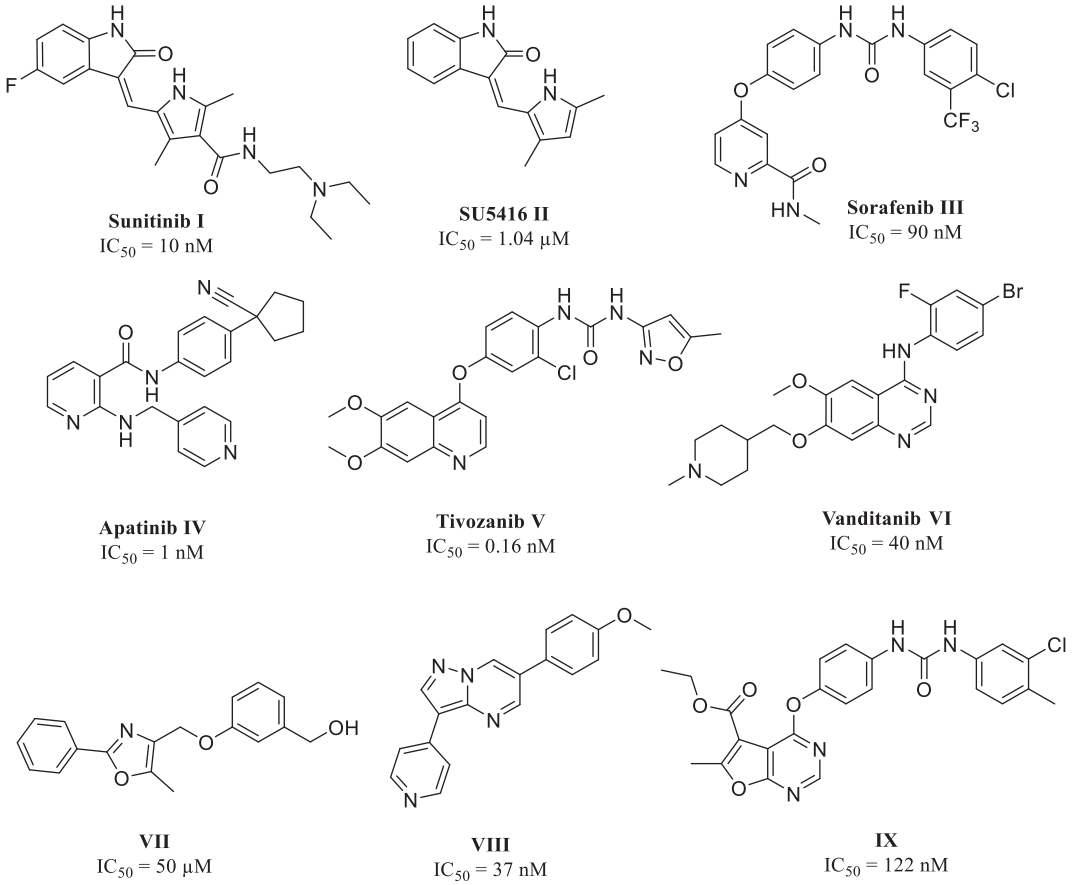

Fig. 1. Representative VEGFR-2 inhibitors.

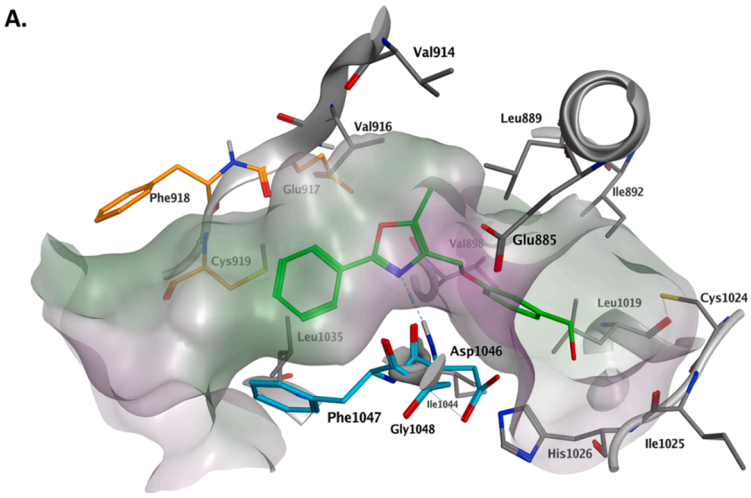

Fig. 2. A. 3D interaction of the co-crystalized oxazole derivative **VII** (green) at the allosteric back pocket of VEGFR-2 (PDB: 3VHK) showing the hinge residues (orange) and the DFG motif (cyan). The hydroxy methylphenyl moiety of **VII** occupies the hydrophobic back pocket and the oxazole nitrogen forms H-bond with Asp1046. The unsubstituted phenyl is in edge to face π-π interaction with Phe1047. **B.** Chemical structure, select calculated physicochemical properties and ligand efficiency of **VII.** Some amino acids are hidden for clarity.

moiety with the premise of reaching out to the hinge residues as with type II inhibitors, (Fig. 3).

Interestingly, the designed triazole derivatives were well aligned with the pyrazolopyrimidine derivative **VIII** previously described as ATP competitive inhibitor of VEGFR-2 (IC_{50} = 37 nM)[24,25], (Fig. 5) giving further support to the rationale behind pursuing the synthesis of the designed compounds. Based on their higher molecular weights and favorable predicted physicochemical properties, these derivatives are anticipated to represent potential small molecule inhibitors of VEGFR-2.

2. Results and discussion

2.1. Chemistry

The synthetic steps adopted for the synthesis of the key intermediates and the final compounds are outlined in Schemes 1-3. Briefly, reaction of phenacyl bromides **1a,b** with malononitrile in the presence of diethyl amine in dimethyl formamide (DMF) furnished 2-amino-5-arylfuran-3-carbonitriles **2a,b**, respectively, as previously reported[30,31]. The key intermediates ethyl-*N*-(3-cyano-5-arylfuran-2-yl)formimidates **3a,b** were prepared via reaction of **2a,b**, respectively, with triethyl orthoformate [32,33] (Scheme 1). Microanalyses and spectral data confirmed the structure of the synthesized compounds. IR spectra of **2a,b** showed stretching bands of NH_2 at 3414, 3325 cm^{-1} and C≡N at 2206 cm^{-1}, whereas these bands were absent in the IR spectra of **3a,b**. ^1H NMR spectra of **2a,b** showed a characteristic singlet signal of CH furan at 6.78 and 6.99 ppm, respectively, along with the D_2O exchangeable singlet signal of NH_2 at 7.48 and 7.61 ppm, respectively. Additionally, **2a** showed the presence of singlet signal at 3.76 ppm assigned for OCH_3 group. On the other hand, **3a,b** showed the typical triplet-quartet pattern of ethyl group at 1.34, 4.39 ppm and 1.35, 4.36 ppm, respectively and the appearance of singlet signal at 8.73 and 8.78 ppm,

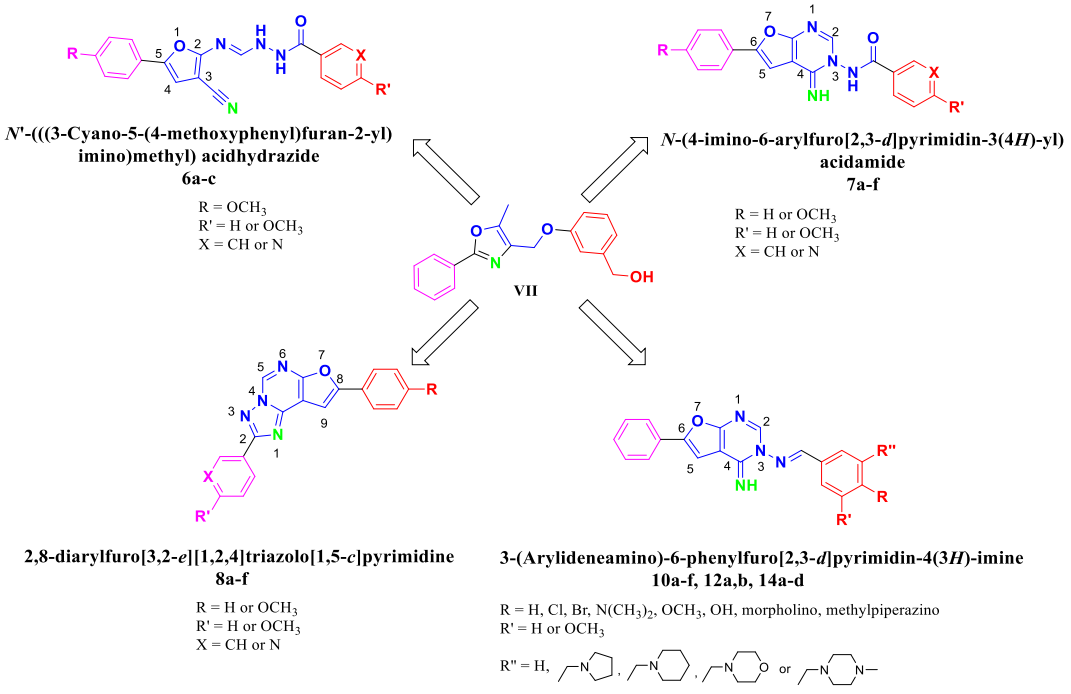

Fig. 3. Essential pharmacophoric features of **VII** and the corresponding features in the designed compounds. The main scaffolds are colored in blue, the H-bond donor/acceptor moieties (green), aromatic moiety hypothesized to occupy the allosteric hydrophobic pocket (red) and the other aromatic moiety pointing towards the hinge region (magenta). (For interpretation of the references to colour in this figure legend, the reader is referred to the web version of this article.)

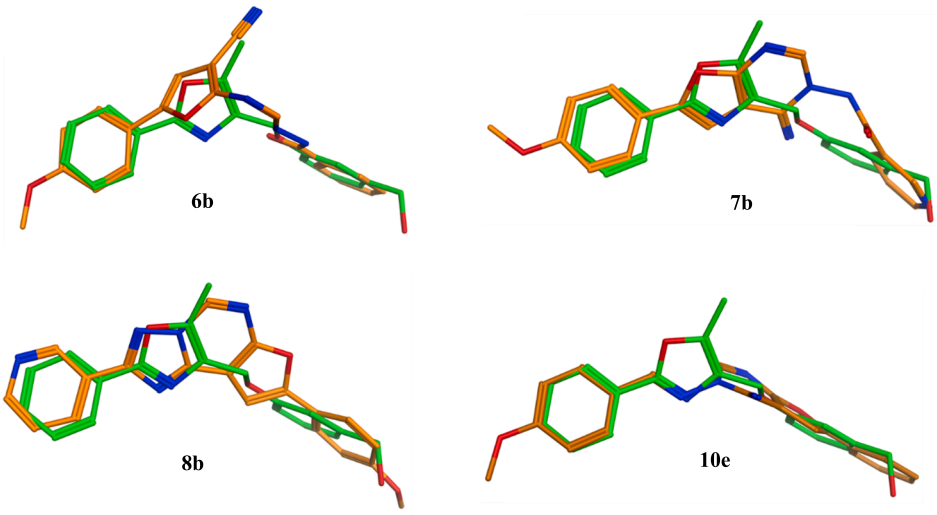

Fig. 4. Alignment of the energy minimized structures of select representatives of the designed compounds (orange) with the 3D bioactive conformer of **VII** (green) extracted from its cocrystal with VEGFR-2 (PDB: **3VHK**). (For interpretation of the references to colour in this figure legend, the reader is referred to the web version of this article.)

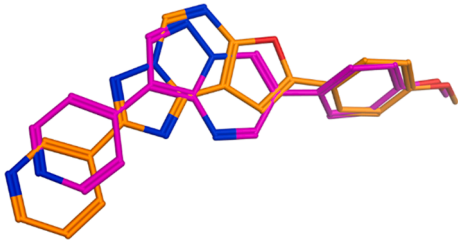

Fig. 5. Alignment of **8b** (orange) with the top docking pose of **VIII** (magenta) at the binding site of VEGFR-2 (PDB: **3VHK**). (For interpretation of the references to colour in this figure legend, the reader is referred to the web version of this article.)

respectively, assigned for HC═N along with the disappearance of NH_2 singlet signal. ^{13}C NMR of **3a,b** showed signals at 14.39 and 14.38 ppm for (—CH_3), 64.47 and 64.59 ppm for (—CH_2) and 159.88 and 159.71 ppm for (O—C═N), respectively. Mass spectrum of **3b** showed a molecular ion peak at *m/z* 240, that matched with its molecular weight.

Esterification of benzoic, nicotinic or 4-methoxybenzoic acids, carried out as reported, using conc. sulfuric acid in the presence of absolute ethanol, provided the corresponding esters **4a-c**[34]. Subsequent hydrazinolysis of **4a-c** using hydrazine hydrate in absolute ethanol provided the acid hydrazides **5a-c**, as reported[34–37]. Reaction of these acid hydrazides with the *p*-methoxyphenyl furan carbonitrile **3a** in absolute ethanol resulted in nucleophilic attack of of the amino group of the acid hydrazide on the electropositive carbon of the imidoester with elimination of ethanol to give *N′*-(((3-cyano-5-(4-methoxyphenyl)furan-2-yl)imino)methyl)-acidhydrazides **6a-c**, respectively. Heating of **6a-c** in boiling DMF resulted in an intramolecular cyclization to provide *N*-(4-imino-6-(4-methoxyphenyl)furo[2,3-*d*]pyrimidin-3(4*H*)-yl)acidamides **7a-c** [38,39]. Contrarily, reaction of **3b** with acid hydrazides in either absolute ethanol or DMF led to the formation of *N*-(4-imino-6-phenyl-furo[2,3-*d*]pyrimidin-3(4*H*)-yl)acidamides **7d-f** directly without formation of the non-cyclized intermediates [38,39]. Boiling of the 4-imino-furo[2,3-*d*]pyrimidines **7a-f** in the high boiling solvent bromobenzene or refluxing **3a,b** with acid hydrazide, directly, in bromobenzene afforded arylfuro[3,2-*e*][1,2,4]triazolo[1,5-*c*]pyrimidines **8a-f**, respectively[38,39] (Scheme 2). Microanalyses and spectral data confirmed the structure of the synthesized compounds. Thus, IR spectra of **6a-c** showed the presence of stretching bands of NH, C≡N and C═O at 3379–3329, 2222–2191 and 1674–1651 cm^{-1}, respectively. ^1H NMR spectra of **6a-c** showed a characteristic singlet signal of OCH_3 at 3.84–3.85 ppm with the appearance of additional singlet signal for compound **6c** at 3.80 ppm assigned to the additional OCH_3 on the other aromatic ring. In addition, two D_2O exchangeable singlet signals of the two NHs appeared at 8.12–8.30 ppm and 9.36–9.42 ppm, respectively, along with a singlet signal at 8.49–8.55 ppm assigned for HC═N. ^{13}C NMR of **6a-c** showed characteristic signals of OCH_3, C≡N, (*N*—C═N) and C═O at 55.86–55.87, 104.32–104.44, 150.53–154.50 and 169.28–170.71 ppm, respectively, with an additional signal of **6c**

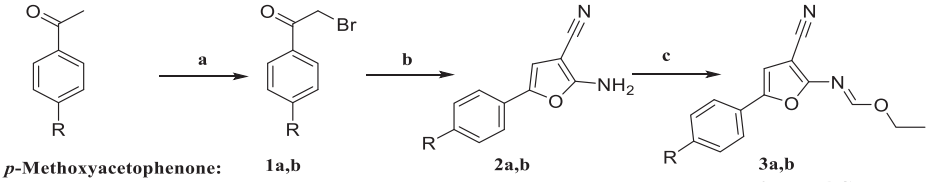

Reagents and conditions

a) NBS, *p*-TsOH, dioxane, stir at rt, overnight.
b) malononitrile, DMF, diethyl amine, stir at 0°C over 30 min then stir at rt, overnight.
c) triethyl orthoformate, reflux, 6h.

Scheme 1. Synthetic pathway to the key intermediates **3a,b**.

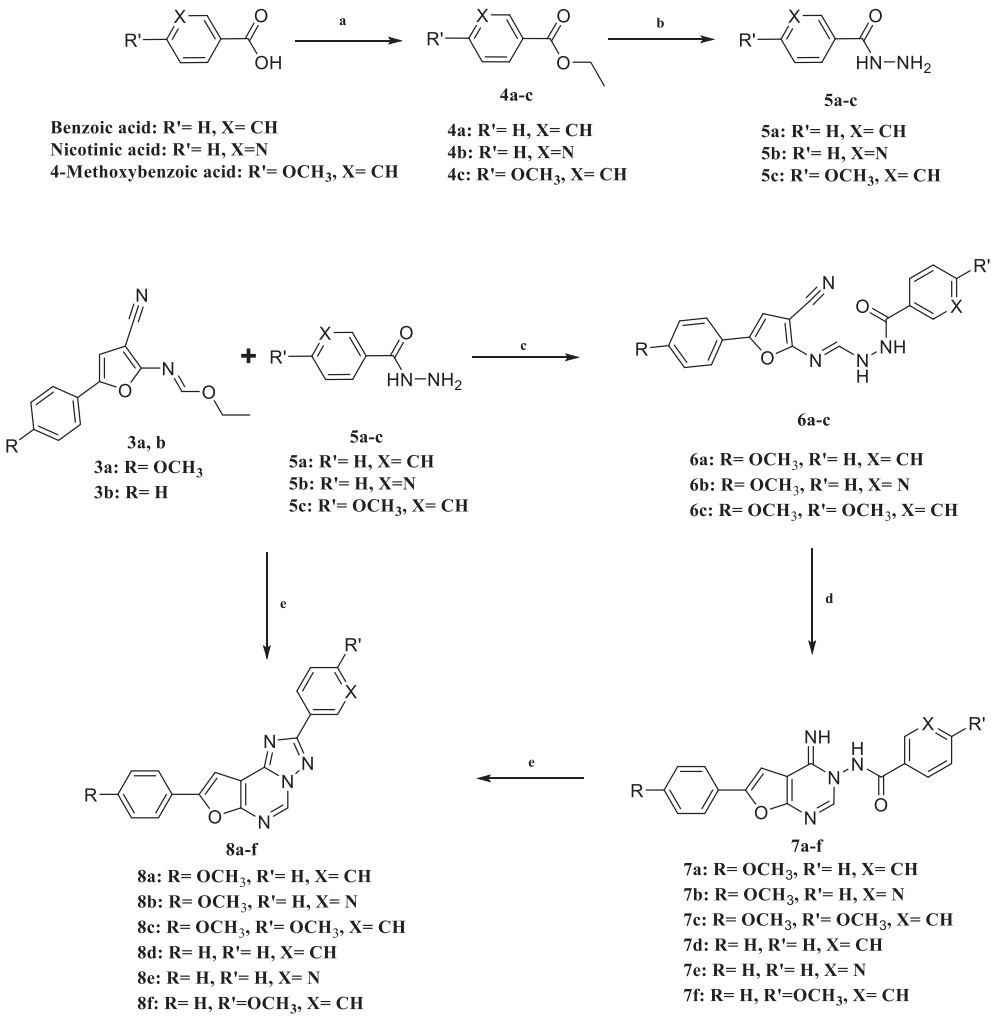

Reagents and conditions

a) conc. H_2SO_4, absolute ethanol, reflux 4h.
b) hydrazine hydrate (99%), absolute ethanol, reflux 4h.
c) absolute ethanol, reflux 1h.
d) DMF, reflux 15 min.
e) bromobenzene, reflux 24h.

Scheme 2. Synthetic pathways to the target compounds **6a-c, 7a-f** and **8a-f**.

(—OCH_3) group at 55.60 ppm. Mass spectrum of **6a** showed a molecular ion peak at *m/z* 360, which revealed the molecular weight of the synthesized compound. On the other hand, The IR spectra of **7a-f** showed NH and C═O stretching bands at 3406–3321 and 1678–1651 cm^{-1}, respectively with no stretching band for C≡N bond. The ^1H NMR spectra of **7a-f** revealed a singlet signal of CH pyrimidine at 8.51–8.67 ppm, in addition to two D_2O exchangeable singlet signals of the two NHs appeared at 8.13–9.62 ppm and 9.40–9.74 ppm. ^{13}C NMR of **7a-f** showed characteristic signals of C═NH and C═O at 160.85–161.46 and 169.30–171.15 ppm, respectively. Mass spectra of **7a** and **7e** showed a molecular ion peak at *m/z* 360 and 331, respectively, which correlates with the molecular weights of these compounds. ^1H NMR spectra of **8a-f** showed a characteristic singlet signal assigned to CH pyrimidine at 9.44–9.73 ppm along with the disappearance of the two D_2O exchangeable singlet signals of NHs that was consistent with their ^{13}C NMR spectra where no signals for C═NH and C═O were detected. The absence of NH and C═O stretching bands in the IR spectra of **8a-f** further confirmed their molecular structures. Mass spectra of **8a** and **8e** showed a molecular ion peak at *m/z* 342 and 314 (M^++1), respectively, as their calculated molecular weights.

The key intermediate 4-imino-6-phenylfuro[2,3-*d*]pyrimidin-3(4*H*)-amine **9** was prepared by hydrazinolysis of -N-(3-cyano-5-phenylfuran-2-yl)formimidate **3b** with hydrazine hydrate in absolute ethanol. Nucleophilic attack of the hydrazine hydrate amino group lone pair on the electropositive carbon of imidoester resulted in its hydrazinolysis with elimination of ethanol. Subsequent intramolecular cyclization took place through nucleophilic attack of the amino group lone pair on the electropositive carbon of C≡N group to give **9** [33,39,40]. IR spectrum of **9** revealed the appearance of NH_2 and NH bands at 3309–3201 cm^{-1} along with the disappearance of C≡N stretching band. ^1H NMR spectra of **9** showed a characteristic singlet signal of CH pyrimidine at 8.21 ppm and two D_2O exchangeable singlet signals of NH_2 and NH at 4.72 and 9.04 ppm, respectively. In addition, ^{13}C NMR of **9** showed a signal corresponding to C═NH at 153.96 ppm along with no signals for CH_2, CH_3, C≡N and (O—C═N). Mass spectrum of **9** showed a molecular ion peak at *m/z* 226. Reaction of **9** with different aromatic aldehydes in the presence of absolute ethanol and catalytic amount of glacial acetic acid resulted in the formation of Schiff's bases, 3-(arylideneamino)-6-

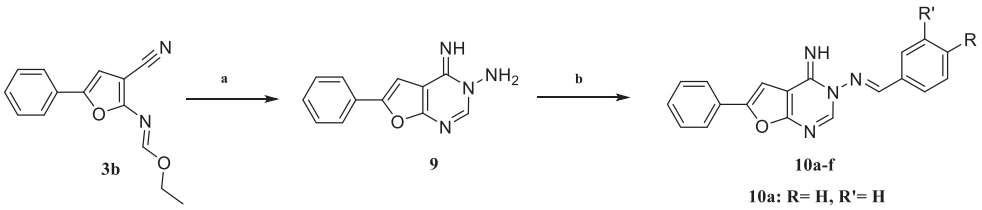

Reagents and conditions
a) hydrazine hydrate (99%), absolute ethanol, reflux, 8h.
b) aromatic aldehyde, absolute ethanol, catalytic glacial acetic acid, reflux, 3h.

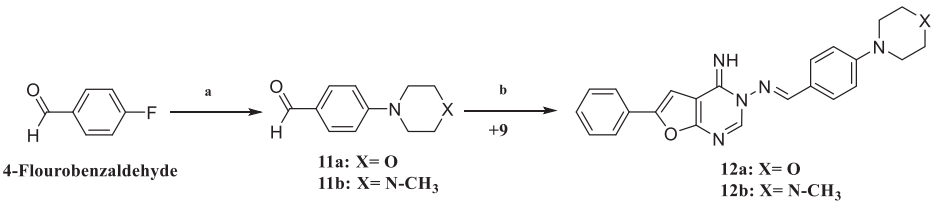

Reagents and conditions
a) morpholine or *N*-methylpiperazine, anhydrous K_2CO_3, dry DMF, reflux, 7h.
b) absolute ethanol, reflux, 4h.

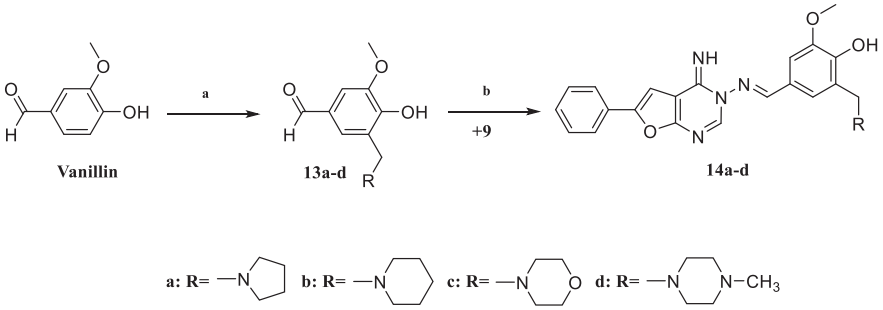

Reagents and conditions
a) formaldehyde (30%), secondary amine, ethanol (70%), reflux 30 min then stir at rt, overnight.
b) absolute ethanol, catalytic glacial acetic acid, reflux 4h.

Scheme 3. Synthetic pathway for the preparation of 3-(arylideneamino)-6-phenylfuro[2,3-*d*]pyrimidin-4(3H)-imine derivatives **10a-f**, **12a,b** and **14a-d.**

phenylfuro[2,3-*d*]pyrimidin-4(3*H*)-imines **10a-f** [41], (Scheme 3). IR spectra of compounds **10a-f** showed NH stretching bands at 3205–3190 cm^{-1} with no NH_2 stretching bands. The phenolic derivative **10f** showed OH stretching band at 3525 cm^{-1}. ^1H NMR spectra of **10a-f** revealed a characteristic singlet signal assigned to N═CH at 8.33–8.40 ppm, in addition to the D_2O exchangeable singlet signal of NH at 11.71–12.05 ppm and the disappearance of the NH_2 signal. Additionally, compound **10d** showed a singlet signal at 3.01 ppm representing $2CH_3$ of *N,N*-dimethyl moiety, while **10e** showed a singlet signal at 3.84 ppm of OCH_3. Also, **10f** showed a singlet signal of OCH_3 at 3.96 ppm and the D_2O exchangeable singlet signal of OH at 9.56 ppm. ^{13}C NMR of **10a-f** showed characteristic signals of (HC═N—N) and C═NH at 156.22–161.20 and 167.59–167.63 ppm, respectively. An additional signal for **10d** at 31.15 ppm representing $2CH_3$ was appeared, while **10e** and **10f** showed a signal of OCH_3 at 55.79 and 55.68 ppm, respectively.

Furthermore, the 4-aminosubstituted benzaldehydes **11a,b** were prepared as reported through reaction of 4-fluorobenzaldehyde with morpholine or *N*-methylpiperazine in the presence of anhydrous potassium carbonate (K_2CO_3) in dry DMF[42–45]. Reaction of **11a,b** with 4-imino-6-phenylfuro[2,3-*d*]pyrimidin-3(4*H*)-amine **9** in absolute ethanol provided 3-((4-aminosubstituted-benzylidene)amino)-6-phenylfuro[2,3-*d*]pyrimidin-4(3*H*)-imine derivatives **12a,b**[41], (Scheme 3). The structures of **12a,b** were confirmed through microanalyses and spectral data. IR spectra of **12a,b** showed no NH_2 stretching bands along with the persistence of the NH stretching band at 3194, 3201 cm^{-1}, respectively ^1H NMR spectra of **12a,b** revealed a singlet signal of N═CH at 8.35 and 8.34 ppm and the D_2O exchangeable singlet signal of NH at 11.78 and 11.79 ppm, respectively, with the disappearance of NH_2 signal. In addition, compounds **12a** showed the characteristic triplet signals of morpholine at 3.23 and 3.76 ppm assigned for $N(CH_2)_2$ and $O(CH_2)_2$, respectively, while **12b** showed the characteristic triplet signals of *N*-methylpiperazine at 2.46 and 3.27 ppm assigned for the two $N(CH_2)_2$ and a singlet signal of CH_3 at 2.24 ppm. ^{13}C NMR of **12a,b** showed characteristic signals of (HC═N—N) at 156.25, 156.23 ppm, respectively, and C═NH at 167.59 ppm. **12a** showed characteristic signal of $N(CH_2)_2$ and $O(CH_2)_2$ of morpholine at 48.03 and 66.44 ppm, respectively, while **12b** revealed signals at 46.21, 47.66 and 54.88 ppm assigned for CH_3 and the two $N(CH_2)_2$, respectively. Mass spectrum of **12a** showed a molecular ion peak at *m/z* 399. Finally, the functionalized aldehydes **13a-d** were prepared as reported by Mannich reaction of vanillin with appropriate secondary amines and 30% formaldehyde in ethanol to produce 4-hydroxy-3-methoxy-5-(substituted-1-ylmethyl) benzaldehyde derivatives **13a-d**[46–49]. Subsequent reaction of 4-imino-6-phenylfuro[2,3-*d*]pyrimidin-3(4H)-amine **9** with **13a-d** in absolute ethanol in the presence of catalytic amount of glacial acetic acid produced 4-(((4-imino-6-phenylfuro[2,3-*d*]pyrimidin-3(4H)-yl)imino) methyl)-2-methoxy-6-(substituted-1-ylmethyl)phenol derivatives **14a-d**, respectively[41], (Scheme 3). Microanalyses and spectral data confirmed the structure of the synthesized compounds. IR spectra of **14a-d** showed stretching bands of OH and NH at 3425–3394 and

3205–3197 cm^{-1}, respectively and the absence of NH_2 stretching bands. ^1H NMR spectra of **14a-d** revealed characteristic signals at 1.45–3.61 ppm assigned for aliphatic protons of piperidinyl, *N*-methylpiperazinyl, morpholinyl and pyrrolidinyl, in addition to singlet signals of N-CH_2 and OCH_3 at 3.68–3.83 ppm and 3.94–3.96 ppm, respectively. Moreover, a singlet signal of N═CH appeared at 8.36 ppm and the D_2O exchangeable singlet signal of NH at 11.85–11.87 ppm along with the disappearance of NH_2 signal. It was noticed that the singlet signal of the phenolic OH could not be identified, instead the signal of the water of DMSO appeared as a broad hump shaped signal at 3.5 ppm, that interestingly appeared as a sharp signal upon deuteration. ^{13}C NMR of **14a-d** showed characteristic signals of aliphatic protons of piperidinyl, *N*-methylpiperazinyl, morpholinyl and pyrrolidinyl at 23.68–66.61 ppm along with signals of OCH_3 and N-CH_2 at 55.68–55.81 and 56.44–60.08 ppm, respectively. In addition, characteristic signals of (HC═N—N) and C═NH at 156.35–156.38 and 167.58–167.64 ppm, respectively. Mass spectrum of **14d** showed a molecular ion peak at *m/z* 472, which correlates with its molecular weight.

2.2. Biological evaluation

2.2.1. VEGFR-2 inhibitory activity and structure activity relationship

All the newly synthesized final compounds were tested using *in vitro* VEGFR-2 inhibitory assay with sorafenib as a reference standard. The VEGFR-2 inhibitory activities of the tested compounds are expressed as IC_{50} (nM) and are presented in Table 1 and 2. All the compounds showed nanomolar inhibitory activity against VEGFR-2 with IC_{50} values ranging from 38.72 to 440.00 nM compared to sorafenib ($IC_{50} = 41.24 \pm 1.9$ nM) and **VII** (IC_{50} = 50 μM)[23]. Furan derivatives **6a** and **6c**, furo[2,3-*d*]pyrimidine derivatives **7f, 10b, 10c** and **10f, 12b**, **14c and 14d** and furo[3,2-*e*][1,2,4]triazolo[1,5-*c*]pyrimidine derivatives **8a-c** exhibited good activity with $IC_{50} < 100$ nM. Two main factors seem to operate affecting the observed activity: a) the conformational rigidity of the molecules imparted by the central scaffold, b) steric and/or electronic effects of substituents in the peripheral aryl rings where these effects appear to be context based. For compounds bearing *p*-methoxyphenyl on the furan ring **6a-c**, **7a-c** and **8a-c**, increasing the rigidity of the central scaffold as in the furotriazolopyrimidine **8a-c** increased the activity especially for **8b** ($IC_{50} = 38.72 \pm 1.7$ nM) and **8c** ($IC_{50} = 57.96 \pm 2.8$ nM). This might be explained by their favorable fit and/or interactions at the hydrophobic back pocket. Specifically, the nitrogen atom of nicotinoyl moiety in **8b** and the additional OCH_3 in **8c** may contribute to favorable interactions with the hydrophobic back pocket and/or solvent molecules at the solvent exposed front of the binding site, which makes them more active than **8a** ($IC_{50} = 83.51 \pm 3.9$ nM). It is worth mentioning that **8b** displayed the highest activity among all the tested derivatives being comparable to sorafenib ($IC_{50} = 41.24 \pm 1.9$ nM). Regarding the *N*′-(((3-cyano-5-(4-methoxyphenyl)furan-2-yl)imino)methyl)-acidhydrazide derivatives **6a-c**, the benzoic acid hydrazide **6a** (R′ = H, X = CH) showed comparable activity (IC_{50} = 57.21 ± 2.6 nM) compared to sorafenib whereas the *p*-methoxy derivative **6c** (R′ = OCH_3, X = CH) was slightly less active ($IC_{50} = 70.04 \pm 3.2$ nM) than **6a** and the nicotinoyl isostere **6b** (R′ = H, X = N) was about three times less active ($IC_{50} = 199.40 \pm 9.1$ nM). The corresponding cyclized furo[2,3-*d*]pyrimidine derivatives **7a-c** were generally two to three times less active compared to their furan counterparts following the same activity trend **7a** (R′ = H, X = CH) > **7c** (R′ = OCH_3, X = CH) > **7b** (R′ = OCH_3, X = N) (IC_{50} 143.30 ± 6.5 nM, 226.90 ± 9.9 nM, 440.00 ± 18.0 nM, respectively). Interestingly, removal of the *p*-methoxy group in **7d-f** generally improved the activity compared to **7a-c** especially for **7f** ($IC_{50} = 43.31 \pm 20$) that was equipotent to sorafenib (IC50 = 41.24 ± 1.9) and one of the most active compounds.

The presence of *p*-methoxybenzohydrazide moiety in furan or furo[2,3-*d*]pyrimidine derivatives as in **6c** ($IC_{50} = 70.04 \pm 3.2$ nM) and **7c** ($IC_{50} = 226.90 \pm 9.9$ nM) led to slight decrease in activity compared to those bearing unsubstituted benzohydrazide moiety, **6a** ($IC_{50} = 57.21 \pm 2.6$ nM) and **7a** (IC_{50} = 143.30 ± 6.5 nM). Contrarily, triazole derivatives **8d-f** having unsubstituted phenyl on furan ring exhibited obvious drop in activity compared to their *p*-methoxy congeners **8a-c.** Lacking interactions with the solvent molecules at the solvent exposed areas of the receptor and being less fitted on the hydrophobic pocket may explain this reduction in activity.

SAR analysis of the tested derivatives **9**, **10a-f**, **12a,b** and **14a-d** presented in Table 2 revealed some interesting findings. Removal of the acidamide moiety as in **9** (IC_{50} = 217.70 ± 9.8 nM) resulted in moderate activity compared to sorafenib (IC_{50} = 41.24 ± 1.9 nM).

Table 1

Inhibitory activity of **6a-c**, **7a-f** and **8a-f** against VEGFR-2 *in vitro*.[a]

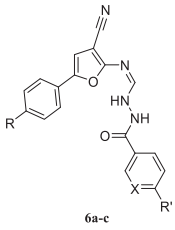

6a-c

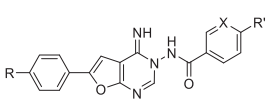

7a-f

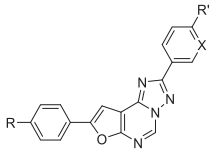

8a-f

Compound	R	R′	X	IC_{50} (nM) ± SD[a]	LE[b]
6a	OCH_3	H	CH	57.21 ± 2.6	0.376
6b	OCH_3	H	N	199.40 ± 9.1	0.347
6c	OCH_3	OCH_3	CH	70.04 ± 3.2	0.345
7a	OCH_3	H	CH	143.30 ± 6.5	0.355
7b	OCH_3	H	N	440.00 ± 18.0	0.330
7c	OCH_3	OCH_3	CH	226.90 ± 9.9	0.321
7d	H	H	CH	134.80 ± 6.2	0.385
7e	H	H	N	244.50 ± 11.0	0.370
7f	H	OCH_3	CH	43.31 ± 2.0	0.382
8a	OCH_3	H	CH	83.51 ± 3.9	0.381
8b	OCH_3	H	N	38.72 ± 1.7	0.399
8c	OCH_3	OCH_3	CH	57.96 ± 2.8	0.362
8d	H	H	CH	156.60 ± 7.0	0.397
8e	H	H	N	417.40 ± 17.0	0.372
8f	H	OCH_3	CH	122.20 ± 5.4	0.372
Sorafenib	–	–	–	41.24 ± 1.9	0.323

[a] Values are means from three independent dose–response curves.

[b] Ligand efficiency (LE) was calculated using the following formula LE = 1.4(−logIC_{50})/HAC) where HAC is the count of heavy atoms [50].

Table 2

Inhibitory activity of **9**, **10a-f**, **12a,b** and **14a-d** against VEGFR-2 *in vitro*.[a]

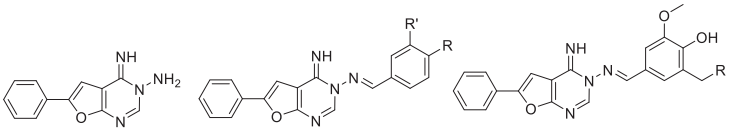

9 **10a-f** **12a,b** **14a-d**

Compound	R	R′	IC_{50} (nM) ± SD[a]	LE[b]
9	–	–	217.70 ± 9.8	0.549
10a	H	H	289.70 ± 12.0	0.381
10b	Cl	H	98.31 ± 4.6	0.392
10c	Br	H	41.40 ± 1.8	0.413
10d	$N(CH_3)_2$	H	132.70 ± 6.0	0.357
10e	OCH_3	H	188.70 ± 8.3	0.362
10f	OH	OCH_3	69.55 ± 3.2	0.371
12a		H	144.60 ± 6.5	0.319
12b	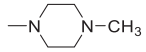	H	76.19 ± 3.5	0.321
14a		–	112.50 ± 5.3	0.295
14b		–	125.00 ± 5.6	0.284
14c		–	51.26 ± 2.4	0.300
14d	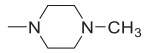	–	85.99 ± 4.1	0.283
Sorafenib	–	–	41.24 ± 1.9	0.323

[a] Values are means from three independent dose–response curves.

[b] Ligand efficiency (LE) was calculated using the following formula LE = 1.4(−logIC_{50})/HAC where HAC is the count of heavy atoms [50].

Replacement of the less rigid planar amide bond in N-(4-imino-6-phenylfuro[2,3-*d*]pyrimidin-3(4H)-yl)acidamide derivatives **7d-f** with the more rigid arylideneamino moiety as in **10a-f** generally enhanced the binding affinity except for the unsubstituted derivative **10a** (IC_{50} = 289.70 ± 12.0 nM). This notion may be attributed to enhanced fitting within the hydrophobic back pocket caused by extra rigidity of the molecule and/or substituent effects. Compounds bearing electron withdrawing moiety as chlorine in **10b** or the bulkier bromine in **10c** showed remarkable increase in activity, especially for **10c** which is one of the most active compounds (IC_{50} = 41.40 ± 1.8 nM) with IC_{50} comparable to that of sorafenib. In contrast, electron donating groups resulted in slight decrease in activity as observed for the dimethylamino and methoxy derivatives **10d** (IC_{50} = 132.70 ± 6 nM) and **10e** (IC_{50} = 188.70 ± 8.3 nM), respectively. The 4-hydroxy-3-methoxy derivative **10f** showed good activity (IC_{50} = 69.55 ± 3.2 nM) that may be explained by the balanced electronic effects of para electron donating phenolic group and the meta-electron withdrawing methoxy group. The 4-morpholino substituted derivative **12a** and its 4-methylpiperazino counterpart **12b** showed IC_{50} of 144.60 ± 6.5 and 76.19 ± 3.5 nM, respectively. Finally, structurally extended Mannich base derivatives **14a-d** showed good activity with IC_{50} values in the range of 51.26–125.00 nM. The good activity of these derivatives may be attributed to the formation of favorable interactions with the protein and/or solvent molecules at the solvent exposed areas of the receptor, especially for **14c** (IC_{50} = 51.26 ± 2.4 nM) and **14d** (IC_{50} = 85.99 ± 4.1 nM. It is worthy to mention that all the tested compounds had higher LE values compared to **VII** ranging from 0.283 to 0.549, Table 1 and 2.

2.2.2. NCI-60 human tumor cell lines screen

Next, we thought to determine if the compounds have direct cytotoxic effects in cancer cells. Thus, the synthesized compounds were submitted to the National Cancer Institute (NCI), USA to be considered for NCI-60 human tumor cell lines screen. Fifteen compounds were selected for screening of their antiproliferative activity using sulforhodamine B assay (SRB) at a single dose of 10 μM. The screening utilizes 60 different human tumor cell lines, representing leukemia, NSCLC, colon, CNS, melanoma, ovarian, renal, prostate and breast cancers. The results are shown in Table 3. Interestingly, the compounds showed no toxicity in the tested cell lines. Since the tested compounds were designed based on a VEGFR-2 specific fragment and VEGFR-2 is mainly expressed in endothelial cells, the lack of cytotoxicity of these compounds suggests target selectivity and encourages further study of the most potent VEGFR-2 inhibitors in human umbilical vein endothelial cells (HUVECs) where VEGFR-2 is highly expressed[51,52].

2.2.3. Antiproliferative activity against HUVECs

Previous studies used inhibition of HUVECs growth as a predictive tool for the antiangiogenic activity *in vitro*[51,52]. Therefore, compounds exhibiting promising VEGFR-2 inhibitory activity **8a-c** and **10c** and sorafenib as a positive control were investigated for their antiproliferative activity against HUVECs using MTT assay. The results are presented in Table 4. The four tested compounds exhibited good cytotoxic activity compared to sorafenib with IC_{50} values in the range of

Table 3
Results of the selected target compounds in the NCI-60 human tumor cell lines screen.

Compound	NCS Number	% Mean Growth	Delta	Range
6a	821,306	100.45	37.80	63.68
6b	821,309	104.67	13.73	34.33
6c	821,312	99.64	34.38	50.96
7a	821,307	103.53	13.15	39.34
7b	821,310	100.28	11.45	29.21
7c	821,313	104.46	9.97	26.24
7d	828,330	100.14	18.77	54.86
7e	828,331	99.55	13.81	38.78
7f	828,334	100.56	21.92	38.38
8a	821,308	101.78	29.98	92.79
8b	821,311	105.49	18.36	36.33
8c	821,314	99.51	46.01	60.86
8d	828,332	102.90	17.85	48.85
8e	828,333	101.62	16.80	37.49
8f	828,335	101.76	12.49	25.30

17.37–61.20 μM. **8b** with the highest VEGFR-2 inhibitory activity among the tested compounds *in vitro*, demonstrated enhanced antiproliferative activity with $IC_{50} = 17.37 \pm 1.03$ μM in comparison to the standard sorafenib ($IC_{50} = 20.64 \pm 1.22$ μM). Moreover, **8c** exhibited comparable antiproliferative activity with sorafenib with $IC_{50} = 22.61 \pm 1.34$ μM. On the other hand, **8a** ($IC_{50} = 39.45 \pm 2.34$ μM) and **10c** ($IC_{50} = 61.20 \pm 3.62$ μM) were moderately active.

2.2.4. Cell cycle analysis and apoptotic effect of 8a-c and 10c on HUVECs

As compounds **8a-c** and **10c** demonstrated good antiproliferative activity against HUVECs, we decided to explore their effects on the cell cycle as well as apoptotic events [52]. Flow cytometric analysis was conducted using annexin V-FITC and propidium iodide double staining of HUVECs incubated with **8a-c** and **10c** at their corresponding IC_{50} values for 48 h. Flow cytometric analysis showed that all the tested compounds increased the population of cells in the pre-G1 phase and the strongest effect was observed with **8b** and **8c**, (Fig. 6). Additionally, **8a** and **8b** caused cell cycle arrest at G2/M phase as evident from the increased fraction of cells in that phase whereas **8c** and **10c** increased the fraction of cells in the G1 phase. Apoptotic events were higher in treated cells compared to the untreated cells and necrotic events were more prominent compared to both early and late apoptosis, (Fig. 7).

2.2.5. Cell invasion and migration assay

Endothelial cells invasion and migration play a key role in tumor angiogenesis[53]. Based on the aforementioned results of antiproliferative activity against HUVECs, the *in vitro* inhibitory effect of compounds **8a-c** and **10c** on invasion and migration of HUVECs was examined. The effect of these compounds on chemotactic migration of HUVECs was measured using cell invasion trans well membrane assay kit (BioVision). This kit utilizes a boyden chamber coated with basement membrane extract, where the cells may invade the matrix and then migrate through a semipermeable membrane in the boyden chamber in response to stimulants or inhibitory compounds[54]. As presented in (Fig. 8), **8c** was equipotent to sorafenib showing potent inhibitory effect on invasion by almost 6.7 folds compared to the control untreated cells. On the other hand, **8b** and **10c** decreased the invasion by nearly 2.7 folds relative to the negative control, while **8a** showed the least decrease by about 2 folds.

Next, wound healing assay was used to further asses the inhibitory effect of the tested compounds on cell migration. This assay includes proprietary "wound field" inserts that create a wound field with a defined gap of 0.9 mm. Migratory cells can extend protrusions and ultimately invade and close the wound field. Healing was inspected after 72 h and the percent of wound closure was determined[55–57]. As presented in (Fig. 9), **8b** demonstrated the greatest inhibitory effect on HUVECs migration being comparable to sorafenib whereas **8a**, **8c** and **10c** showed good inhibition but slightly lower than sorafenib.

2.3. Molecular docking and drug-likeness study

Docking of **8a-c** and **10c** at the binding site of VEGFR-2 was carried out to highlight their potential binding modes. While these compounds were designed initially as type III inhibitors with the potential to act as type II inhibitors, their binding as VEGFR-2 type I inhibitors cannot be completely rolled out given the structural similarity between **VIII** and the triazole derivatives. Thus, the co-crystal structures of VEGFR-2 in complex with sunitinib **I** (PDB: 4AGD)[58], sorafenib **III** (PDB: 3WZE)[59] and **VII** (PDB:3VHK)[23], respectively were downloaded from the protein data bank. VEGFR-2 adopts the "DFG-in" conformation in its complex with sunitinib (PDB: 4AGD)[58], whereas both 3WZE[59] and 3VHK[23] represents the inactive "DFG-out" conformation. VEGFR-2 appears to adopt nearly identical conformation in these two PDB files as judged by the root mean square deviation (RMSD) value of 0.975 for the aligned backbone alpha carbons of the common 302 residues. Interestingly, RMSD value calculated for the 29 pocket residues was 0.341 for the aligned backbone alpha carbons and 0.568 considering all atoms of the pocket. The docking protocol was validated by redocking of the co-crystalized ligands into their corresponding crystal structures. RMSD values and binding scores (S) of the top docking poses are presented in Table 1S and Fig. 50S**.** In each case, the coordinates of the docking pose were in excellent agreement with the coordinates of the co-crystalized ligand with RMSD values < 1 suggesting the validity of the docking protocol. Next, we cross-docked sorafenib **III** and **VII** at the binding site of VEGFR-2 in 3VHK[23] and 3WZE[59], respectively. **VIII** was docked at the active site in the three downloaded cocrystal structures. Only, productive poses that agree with published co-crystal structures or previous modeling studies were considered, and their docking scores are summarized in table 5.

Docking pose of sorafenib **III** into the binding site of VEGFR-2 in complex with **VII** (PDB: 3VHK)[23] agreed with its own cocrystal with VEGFR-2 (PDB: 3WZE) [59], however with apparent less favored binding score ($S = 88.62$ kcal/mol vs. -10.38 kcal/mol). On the other hand, the docking pose of **VII** was slightly more favored in terms of docking score using its own crystal structure (PDB: 3VHK)[23] compared to sorafenib cocrystal structure (PDB: 3WZE) [59]. Previous modeling studies of **VIII** suggested that its pyrazolo N1 forms H-bond to the hinge Cys919 at the adenine binding site whereas its 4-methoxy phenyl is positioned at the entry of the narrow hydrophobic back pocket[24,25]. **VIII** docking at binding site of VEGFR-2 in all the three crystal structures agreed with the previous modeling studies with docking score of -6.93, -7.48 and -7.30 kcal/mol at 4AGD[58], 3VHK [23] and 3WZE[59], respectively. These docking scores suggest less favored binding of **VIII** compared to **VII** despite their huge difference in binding affinities (24 nM vs 50 μM, respectively). Thus, docking scores seems not completely satisfactory to explain the observed VEGFR-2 inhibitory activities of the tested compounds in detail. Nevertheless, a useful general insight about the potential binding modes might still be provided. Correlating with their higher binding affinities compared to other tested derivatives, triazole derivatives **8a-c** had higher docking scores (data not shown). Triazole derivatives **8a-c** occupied the allosteric back pocket adopting a binding mode similar to **VII** in docking experiments involving VEGFR-2 with DFG-out conformation. For instance, N1 of the triazole ring in **8c** formed HB with Asp1046 at the DFG motif and the triazolo pyrimidine ring system was engaged in distance dependent interaction with Lys868 whereas the 2-aryl moiety was buried deep at the back pocket mimicking the hydroxy methylphenyl moiety in **VII**. Lack of favorable hydrophobic interactions offered by the *p*-methoxy group on this ring specially with Leu1019 appears to contribute to the lower binding affinities of **8a** compared to **8c**. Moreover, the 8-aryl ring was pointing out towards the hinge region where the *p*-methoxy group in **8c** had several hydrophobic interactions to Phe1047 at the DFG motif and Leu840 and Val848 and was within HB distance to the backbone amine functionality of Cys919, (Fig. 10). On the other hand, **10c** was engaged in HB with Asp1046 at the DFG-out motif through the N of the arylideneamino group. Additionally, the furo[2,3-*d*]pyrimidine ring contributed to distance dependent interactions with Lys 868, Val 916 and Leu 1035 and arene-H interactions with Phe1047 at the DFG motif and Val848. Besides, the 6-phenyl ring was engaged in pi-pi interaction with Phe918, (Fig. 11).

Interestingly, using VEGFR-2 DFG-in confirmation (PDB: 4AGD) [58], docking poses of **8a-c** that mimics **VIII** top docking pose were observed. However, the docking scores were only marginally improved compared to **VIII** and less favored than sunitinib **I.**

Finally, the drug-likeness profiles for **8a-c** and **10c** were predicted using SwissADME server[60]. Sunitinib **I,** sorafenib **III, VII** and **VIII** were included for comparison. **8a-c and 10c** showed no violation to Lipinski, Ghose, Veber, Egan and Muegge pharmacokinetics filters, and exhibited no alerts for Pan Assay Interfering Substances (PAINS) as presented in Table 2S. Additionally, they displayed a predicted consensus logPo/w value within the range of 2.86–4.13 along with moderate water solubility, high GIT absorption and all are not P-gp

Table 4

Antiproliferative activity of **8a-c** and **10c** against HUVECs.[a]

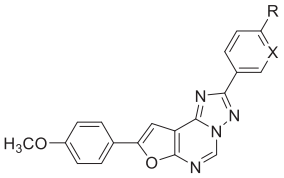

8a: R=H, X= CH
8b: R= H, X= N
8c: R= OCH_3, X= CH

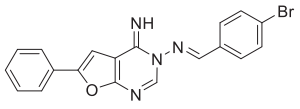

10c

Compound	IC_{50} (μM) ± SD
8a	39.45 ± 2.34
8b	17.37 ± 1.03
8c	22.61 ± 1.34
10c	61.20 ± 3.62
Sorafenib	20.64 ± 1.22

[a] Values are mean from three independent dose–response curves.

substrates. Furthermore, the oral bioavailability radar chart of **8a-c** and **10c** indicated their good predicted oral bioavailability with the same predicted bioavailability score of sunitinib and sorafenib.

3. Conclusion

Series of novel furan **6a-c**, furo[2,3-*d*]pyrimidine **7a-f**, **9**, **10a-f**, **12a, b**, **14a-d** and furo[3,2-*e*][1,2,4]triazolo[1,5-*c*]pyrimidine **8a-f** derivatives were designed and synthesized as inhibitors of VEGFR-2. The synthesized compounds showed different inhibitory activity against VEGFR-2 *in vitro* with IC_{50} in the range of 38.72–440.00 nM in comparison to sorafenib (IC_{50} = 41.24 nM). 8-(4-Methoxyphenyl)-2-arylfuro[3,2-*e*][1,2,4]triazolo[1,5-*c*]pyrimidine derivatives **8a-c** exhibited stronger inhibitory effects than their 8-phenyl counterparts **8d-f** and **8b** (IC_{50} = 38.72 ± 1.7 nM) was more potent compared to sorafenib. Furan derivatives **6a-c** showed superior inhibitory activity compared to their corresponding furo[2,3-*d*]pyrimidine derivatives **7a-c**. Surprisingly, compound **7f** (IC_{50} = 43.31 nM) was the only *N*-(4-imino-6-arylfuro[2,3-*d*]pyrimidin-3(4*H*)-yl)acidamide derivative that showed good inhibitory activity against VEGFR-2. The furo[2,3-*d*]pyrimidine derivatives possessing electron withdrawing moieties **10b**, **10c** and **10f** (IC_{50} = 98.31, 41.40 and 69.55 nM, respectively) were among the most active compounds. Also, substituted amino substituents as in **12b**, **14c** and **14d** (IC_{50} = 76.19, 51.26 and 85.99 nM, respectively) enhanced the activity possibly due to formation of favorable interactions with the solvent molecules at the solvent exposed areas of the receptor. Fifteen derivatives were selected for testing in the NCI 60 cell line screening assay where they showed no antiproliferative effects at 10 μM. Inhibition of human umbilical vein endothelial cells (HUVECs) was used as a predictive tool for the antiangiogenic activity *in vitro*. Accordingly, compounds exhibiting promising VEGFR-2 inhibitory activity **8a-c** and **10c** were further investigated for their antiproliferative activity against HUVECs using MTT assay. **8b** demonstrated enhanced antiproliferative activity with IC_{50} = 17.37 ± 1.03 μM compared to sorafenib (IC_{50} = 20.64 ± 1.22 μM). Moreover, compound **8c** exhibited comparable antiproliferative activity with sorafenib (IC_{50} = 22.61 ± 1.34 μM). On the other hand, **8a** and **10c** were moderately active. In addition, **8a** and **8b** caused cell cycle arrest at G2/M phase in HUVECs and **8b** showed the strongest effects on the total apoptotic events, while **8c** and **10c** mainly affected cell cycle at G1 phase. Furthermore, these compounds exhibited good inhibition of HUVECs invasion and migration compared to positive (sorafenib) and negative controls. Docking and drug likeness study suggested that compound **8a-c** and **10c** are probably acting as type III VEGFR-2 inhibitors through fitting the allosteric hydrophobic pocket of the DFG-out conformation. They displayed favorable predicted pharmacokinetic properties and predicted oral bioavailability score that was comparable to sorafenib and sunitinib. Consequently, compounds **8a-c** and **10c** represent promising starting points towards type VEGFR-2 inhibitors with enhanced ligand efficiency compared to **VII**.

4. Experimental

4.1. Chemistry

Melting points were determined by open capillary tube method on Electrothermal Stuart SMP_3 digital melting point apparatus and are uncorrected. Elemental microanalyses were performed at the Regional Center for Mycology and Biotechnology, Al-Azhar University. Infrared spectra were determined using Shimadzu Infrared spectrometer (IR-435), Faculty of Pharmacy, Cairo University and expressed in wave number (cm^{-1}), using potassium bromide discs. ^{1}H NMR spectra were performed in DMSO-d_6 using Bruker, 400 MHz NMR spectrometer, Microanalytical unit, Faculty of Pharmacy, Cairo University. ^{13}C NMR spectra were recorded using Bruker, 100 MHz NMR spectrometer, Microanalytical unit, Faculty of Pharmacy, Cairo University. Mass spectra were performed at the Regional Center for Mycology and Biotechnology, Al-Azhar University. Thin layer chromatography was performed using silica gel/TLC cards DC-Alufolien-Kiesel gel (Vilber GmbH, Germany) with fluorescent indicator UV254 using chloroform: methanol 9.5: 0.5 as the eluting system and the spots were visualized using Vilber Lourmet ultraviolet lamp (Vilber GmbH, Germany) at λ = 254 nm. Compounds **1a,b**[61–63], **2a,b**[30], **4a-c**[34], **5a-c**[34–37], **11a,b**[42–45], **13a-d**[46–49] were prepared according to their reported procedures.

4.1.1. General procedure for preparation of *3a,b*

Triethyl orthoformate (5 ml/g) was heated with either **2a** or **b** (10 mmol) under reflux conditions for 6 h. The reaction mixture was evaporated to the least amount and left overnight for complete evaporation. The obtained dry solid was crystallized from methanol to give **3a,b**, respectively.

4.1.1.1. Ethyl-N-(3-cyano-5-(4-methoxyphenyl)furan-2-yl)formimidate (3a). Brown powder; yield, 64%; m.p., 125–127 °C; IR (KBr) $\nu_{max.}$/cm^{-1}: 3120 (CH aromatic), 2978 (CH aliphatic), 2222 (C≡N), 1504 (C=C aromatic). ^{1}H NMR (DMSO-d_6 D2O) δ: 1.34 (t, J = 7.10, 3H, CH_3), 3.79 (s, 3H, OCH_3), 4.39 (q, J = 6.95, 2H, CH_2), 6.99 (d, J = 8.88, 2H, Ar-H), 7.13 (s, 1H, CH furan), 7.66 (d, J = 8.84, 2H, Ar-H), 8.73 (s, 1H, HC=N). ^{13}C NMR (DMSO-d_6) δ: 14.39 (—CH_3), 55.73 (—OCH_3), 64.47 (—CH_2), 85.38 (—C—C≡N), 105.42 (—C≡N), 114.86, 121.84, 124.15, 125.72, 148.95, 159.11, 161.44 (Ar-Cs), 159.88 (O—C=N). Anal. Calcd. for $C_{15}H_{14}N_2O_3$ (270.29): C, 66.66; H, 5.22; N, 10.36. Found: C, 66.43;

H, 5.40; N, 10.59.

4.1.1.2. Ethyl-N-(3-cyano-5-phenylfuran-2-yl)formimidate ***(3b)***. Light brown powder; yield, 80%; m.p., 120–121 °C; IR (KBr) $\nu_{max.}/cm^{-1}$: 3124 (CH aromatic), 2974 (CH aliphatic), 2222 (C≡N), 1562 (C=C aromatic). ^{1}H NMR (DMSO-d_6 D2O) δ: 1.35 (t, J = 7.08, 3H, CH_3), 4.36 (q, J = 7.07, 2H, CH_2), 7.35 (t, J = 7.30, 2H, Ar-H and CH furan), 7.46 (t, J = 7.62, 2H, Ar-H), 7.74 (d, J = 7.36, 2H, Ar-H), 8.78 (s, 1H, HC=N). ^{13}C NMR (DMSO-d_6) δ: 14.38 (—CH_3), 64.59 (—CH_2), 85.48 (—**C**—C≡N), 107.41 (—C≡N), 114.54, 124.04, 128.81, 129.06, 129.38, 148.68, 161.87 (Ar-C*s*), 159.71 (O—C=N). Ms, *m/z* (%): 240 (M^+, 16.56). Anal. Calcd. for $C_{14}H_{12}N_2O_2$ (240.26): C, 69.99; H, 5.03; N, 11.66. Found: C, 70.13; H, 5.19; N, 11.87.

4.1.2. General procedure for preparation of compounds ***6a-c***

Equimolar amounts of ethyl-N-(3-cyano-5-(4-methoxyphenyl)furan-2-yl)formimidate **3a** and acid hydrazide derivative **5a-c** (10 mmol) in absolute ethanol (5 ml) were heated under reflux for 1 h. The obtained solid was filtered while hot washed with ethanol, dried to give **6a-c**, respectively.

4.1.2.1. N′-(((3-Cyano-5-(4-methoxyphenyl)furan-2-yl)imino)methyl)-benzohydrazide ***(6a)***. Buff powder; yield, 54%; m.p., 277–279 °C; IR (KBr) $\nu_{max.}/cm^{-1}$: 3329 ($NH_{(s)}$), 3051 (CH aromatic), 2958 (CH aliphatic), 2191 (C≡N), 1651 (C=O), 1612 (NH bending), 1558, 1504 (C=C aromatic). ^{1}H NMR (DMSO-d_6 D2O) δ: 3.85 (s, 3H, OCH_3), 7.11 (d, J = 8.60, 2H, Ar-H), 7.38–7.43 (m, 4H, Ar-H and CH furan), 7.78 (d, J = 8.72, 2H, Ar-H), 8.12–8.14 (m, 2H, Ar-H and 1H, NH, D_2O exchangeable), 8.50 (s, 1H, HC=N), 9.39 (s, 1H, NH, D_2O exchangeable). ^{13}C NMR (DMSO-d_6) δ: 55.87 (—OCH_3), 98.50 (—**C**—C≡N), 104.36 (—C≡N), 115.32, 121.25, 126.79, 127.82, 128.52, 129.94, 138.43, 149.32, 154.42, 160.87 (Ar-C*s*), 150.53 (*N*—C=N), 170.71 (C=O). Ms, *m/z* (%): 360 (M^+, 29.42), 361 (M^++1, 29.27). Anal. Calcd. for $C_{20}H_{16}N_4O_3$ (360.37): C, 66.66; H, 4.48; N, 15.55. Found: C, 66.57; H, 4.63; N, 15.68.

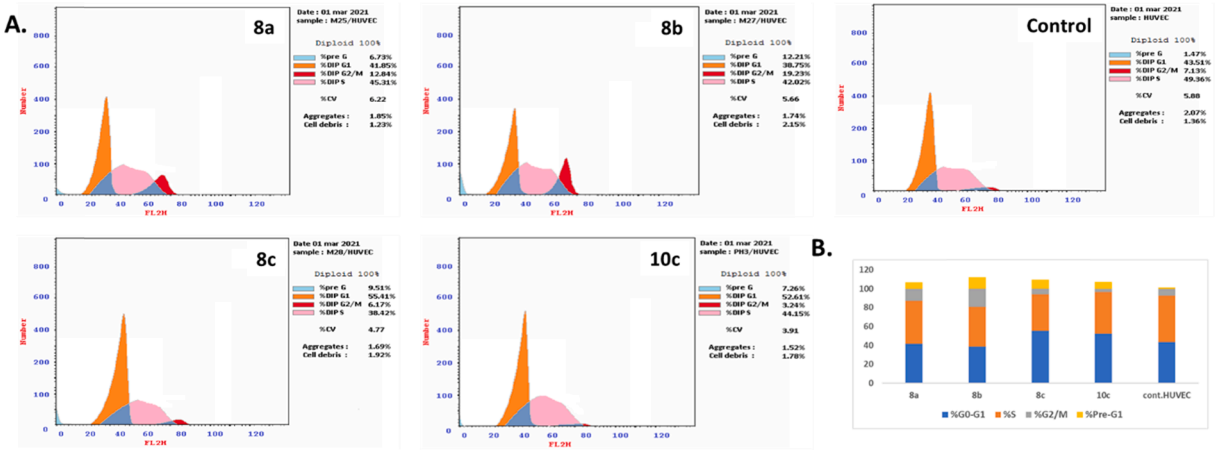

Fig. 6. Effect of **8a-c** or **10c** on HUVECs cell cycle compared to negative control. **A.** Flow cytometric cell cycle analysis of HUVECs treated with **8a-c** or **10c** at their corresponding IC_{50} values for 48 h. **B.** Quantification of the different cell cycle phases of HUVECs treated with **8a-c** or **10c** for 48 h.

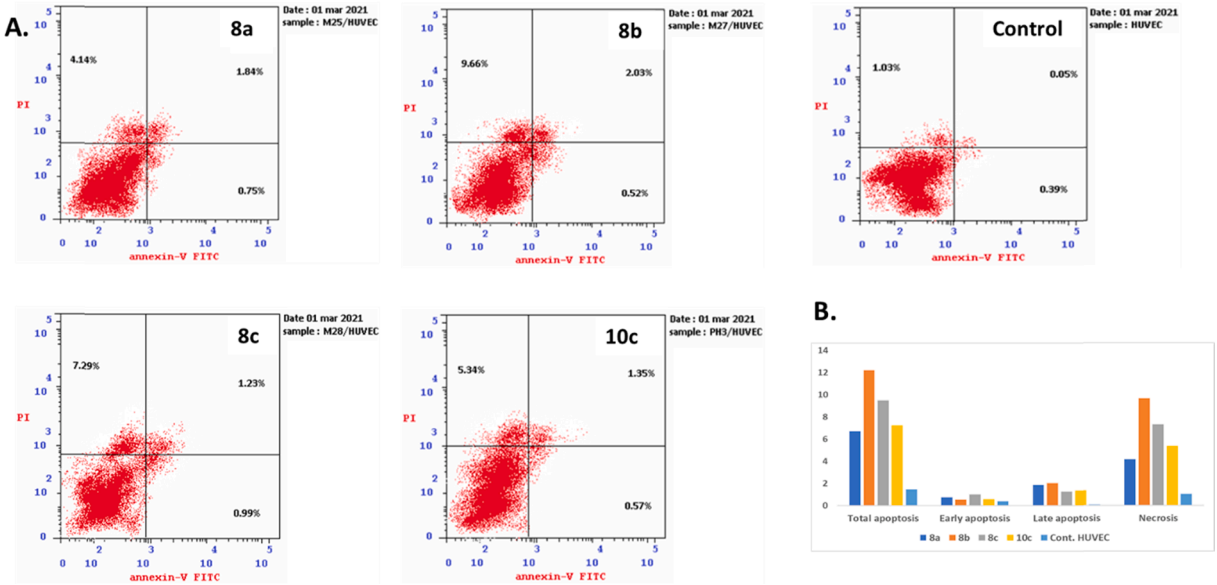

Fig. 7. A. Annexin V-FITC and propidium iodide double staining of HUVECs incubated with **8a-c** and **10c** at their corresponding IC_{50} values for 48 h. **B.** Summary of the apoptotic and necrotic effects of **8a-c** and **10c** in HUVECs.

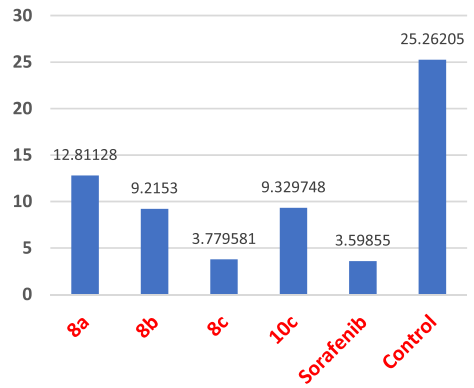

Fig. 8. The effect of compounds **8a-c** and **10c** on chemotactic migration of HUVECs using trans well membrane assay kit compared to negative control and positive control (sorafenib).

4.1.2.2. N′-(((3-Cyano-5-(4-methoxyphenyl)furan-2-yl)imino)methyl)-3-pyridinohydrazide ***(6b)***. Light brown powder; yield, 65%; m.p., 297–299 °C; IR (KBr) $\nu_{max.}/cm^{-1}$: 3379 ($NH_{(s)}$), 3101, 3074 (CH aromatic), 2970 (CH aliphatic), 2222(C≡N), 1674 (C═O), 1635 (NH bending), 1593, 1546, 1504 (C═C aromatic). ^{1}H NMR (DMSO-d_6 D2O) δ: 3.84 (s, 3H, OCH_3), 7.11 (d, J = 8.92, 2H, Ar-H), 7.42–7.45 (m, 2H, Ar-H of pyridine and CH furan), 7.78 (d, J = 8.84, 2H, Ar-H), 8.30 (s, 1H, NH, D_2O exchangeable), 8.38 (dt, J = 1.90, 7.84, 1H, Ar-H of pyridine), 8.55 (s, 1H, HC═N), 8.62 (dd, J = 4.78, 1.74, 1H, Ar-H of pyridine), 9.29 (d, J = 1.28, 1H, Ar-H of pyridine), 9.42 (s, 1H, NH, D_2O exchangeable). ^{13}C NMR (DMSO-d_6) δ: 55.86 (—OCH_3), 98.48 (—C—C≡N), 104.44 (—C≡N), 115.32, 121.20, 123.27, 125.73, 126.81, 133.61, 135.83, 147.46, 149.13, 149.97, 159.89, 160.89 (Ar-Cs), 154.50 (*N*—C═N), 169.28 (C═O). Anal. Calcd. for $C_{19}H_{15}N_5O_3$ (361.36): C, 63.15; H, 4.18; N, 19.38. Found: C, C, 63.49; H, 4.26; N, 19.57.

4.1.2.3. N′-(((3-Cyano-5-(4-methoxyphenyl)furan-2-yl)imino)methyl)-4-methoxybenzohydrazide ***(6c)***. Creamy white powder; yield, 60%; m.p., > 300 °C; IR (KBr) $\nu_{max.}/cm^{-1}$: 3329 ($NH_{(s)}$), 3070 (CH aromatic), 2954 (CH aliphatic), 2191 (C≡N), 1651 (C═O), 1612 (NH bending), 1562, 1504 (C═C aromatic). ^{1}H NMR (DMSO-d_6 D2O) δ: 3.80 (s, 3H, OCH_3), 3.85 (s, 3H, OCH_3), 6.92 (d, J = 8.48, 2H, Ar-H), 7.12 (d, J = 8.56, 2H, Ar-H), 7.43 (s, 1H, CH furan), 7.78 (d, J = 8.56, 2H, Ar-H), 8.06 (d, J =

Table 5
Results of docking experiments for **8a-c, 10c, sunitinib I, sorafenib III, VII** and **VIII** at the active site of VEGFR-2 (PDB files: 4AGD, 3WZE and 3VHK)

Compound	Docking Score at 4AGD (Kcal/mol)	Docking Score at 3WZE (Kcal/mol)	Docking Score 3VHK (Kcal/mol)
8a	−6.98	−8.02	−7.71
8b	−6.98	−8.00	−7.62
8c	−7.26	−8.47	−8.16
10c	−6.23	−7.58	−7.78
Sunitinib	−8.26[a]	ND	ND
Sorafenib	ND	−10.38[a]	−8.62
VII	ND	−7.56	−8.08[a]
VIII	−6.93	−7.30	−7.48

[a] Self-docking experiment.

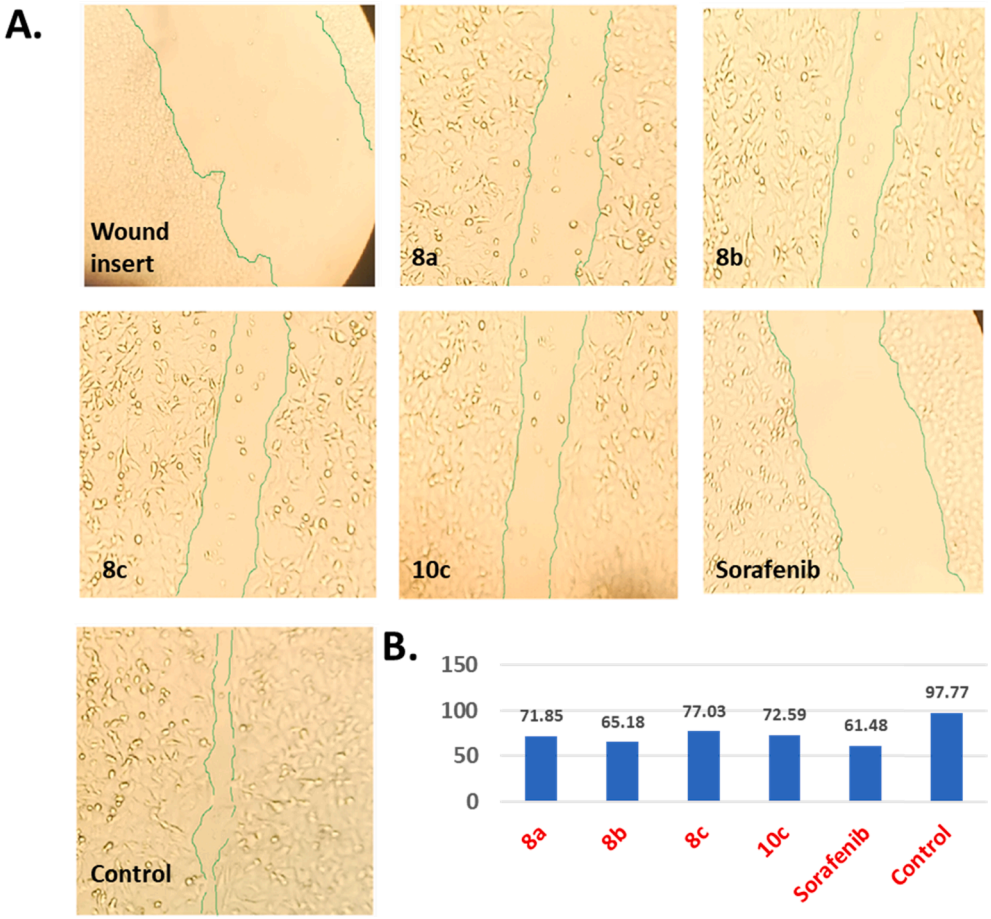

Fig. 9. Wound healing assay. **A.** Microscopic images illustrating the inhibitory effect of **8a-c** and **10c** on the migration of HUVECs in comparison with sorafenib (positive control) and negative control. **B.** % Closure of induced wounds in HUVECs in response to migration inhibition.

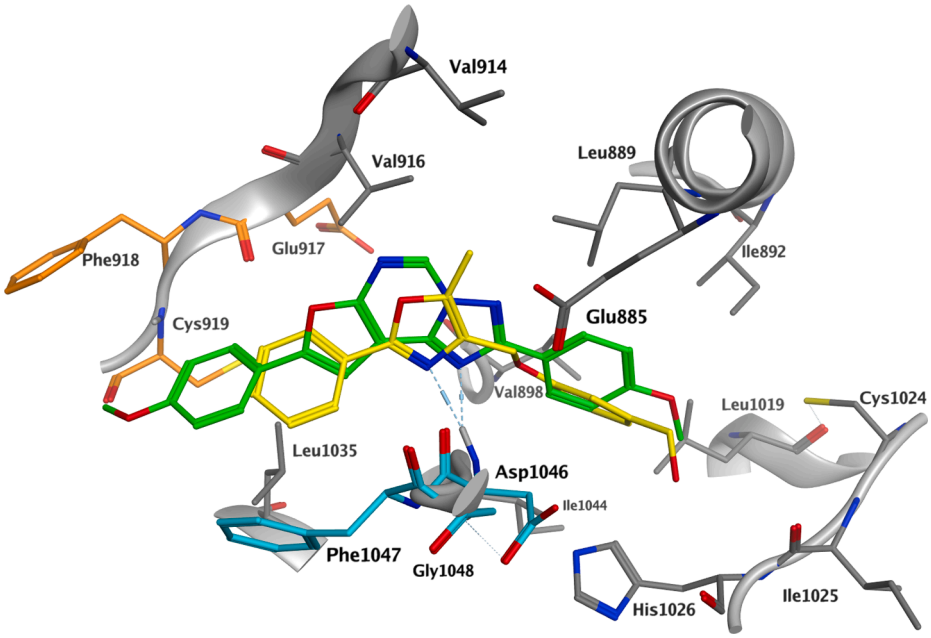

Fig. 10. The top docking pose of **8c** (green) superimposed on the co-crystalized **VII** (yellow) at the binding site of VEGFR-2 (PDB: 3VHK) illustrating the hinge residues (orange) and the DFG motif (cyan). Some amino acids are hidden for clarity. (For interpretation of the references to colour in this figure legend, the reader is referred to the web version of this article.)

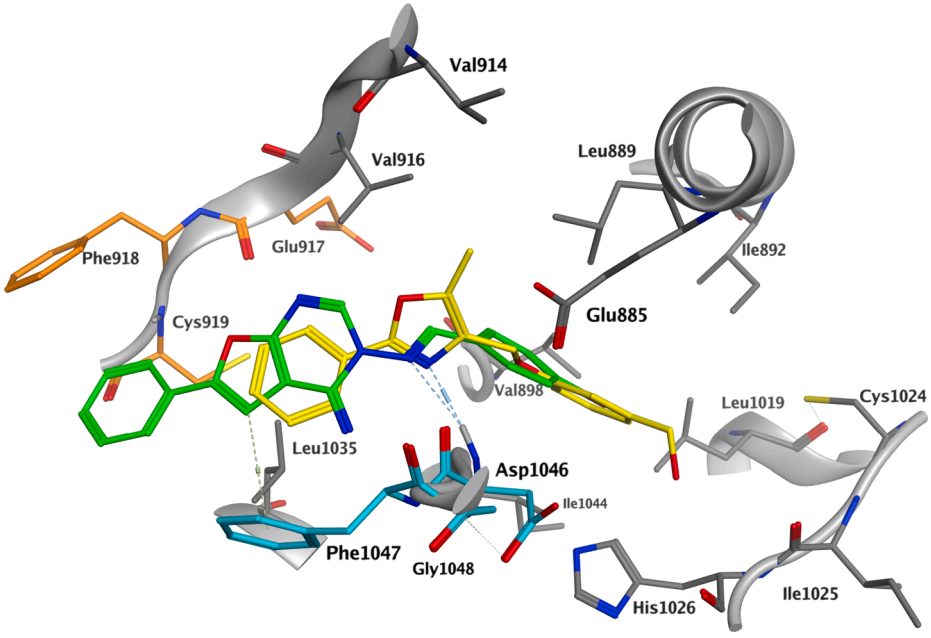

Fig. 11. The top docking pose of **10c** (green) superimposed on the co-crystalized **VII** (yellow) at the binding site of VEGFR-2 (PDB: 3VHK) illustrating the hinge residues (orange) and the DFG motif (cyan). Some amino acids are hidden for clarity. (For interpretation of the references to colour in this figure legend, the reader is referred to the web version of this article.)

8.48, 2H, Ar-H), 8.16 (s, 1H, NH, D_2O exchangeable), 8.49 (s, 1H, HC═N), 9.36 (s, 1H, NH, D_2O exchangeable). ^{13}C NMR (DMSO-d_6) δ: 55.60, 55.87 (2 OCH_3), 98.51 (—**C**—C≡N), 104.32 (—C≡N), 113.06, 115.32, 121.27, 126.77, 130.07, 131.02, 149.46, 154.36, 160.85 (Ar-C*s*), 150.58 (*N*—C═N), 170.42 (C═O). Anal. Calcd. for $C_{21}H_{18}N_4O_4$ (390.40): C, 64.61; H, 4.65; N, 14.35. Found: C, 64.89; H, 4.76; N, 14.52.

*4.1.3. Synthesis of compounds **7a-f***

*4.1.3.1. General procedure for preparation of compounds **7a-c.***

Compounds **6a-c** (10 mmol) in dry dimethyl formamide (DMF) (5 ml) were heated under reflux for 15 min, cooled to 0 °C. The obtained solid was filtered and washed with hexane, dried to give **7a-c**, respectively.

*4.1.3.1.1. N-(4-Imino-6-(4-methoxyphenyl)furo[2,3-d]pyrimidin-3 (4H)-yl)benzamide **(7a)**.* Shiny creamy white powder; yield, 70%; m.p., 284–285 °C; IR (KBr) $\nu_{max.}$/cm^{-1}: 3336 ($NH_{(s)}$), 3055 (CH aromatic), 2931 (CH aliphatic), 1654 (C═O), 1608 (NH bending), 1539, 1500, 1462 (C═C aromatic). ^{1}H NMR (DMSO-d_6 D2O) δ: 3.85 (s, 3H, OCH_3), 7.12 (d, J = 8.52, 2H, Ar-H), 7.39–7.44 (m, 4H, Ar-H and CH furan), 7.79 (d, J = 8.56, 2H, Ar-H), 8.13–8.15 (m, 2H, Ar-H and 1H, NH, D_2O

exchangeable), 8.51 (s, 1H, CH pyrimidine), 9.40 (s, 1H, NH, D_2O exchangeable). ^{13}C NMR (DMSO-d_6) δ: 55.83 (—OCH_3), 98.38, 104.43, 115.26, 121.13, 126.78, 127.92, 128.54, 130.16, 137.99, 149.03,150.53, 154.55 (Ar-C*s*), 160.85 (—C═NH), 171.15 (C═O). Ms, *m/z* (%): 360 (M^+, 16.80). Anal. Calcd. for $C_{20}H_{16}N_4O_3$ (360.37): C, 66.66; H, 4.48; N, 15.55. Found: C, 66.78; H, 4.67; N, 15.73.

4.1.3.1.2. N-(4-Imino-6-(4-methoxyphenyl)furo[2,3-d]pyrimidin-3 (4H)-yl)-3-pyridinamide ***(7b)***. Creamy white powder; yield, 72%; m.p., > 300 °C; IR (KBr) $\nu_{max.}$/cm^{-1}: 3329 ($NH_{(s)}$), 3086 (CH aromatic), 2931 (CH aliphatic), 1654 (C═O), 1612 (NH bending), 1589, 1543, 1504 (C═C aromatic). ^1H NMR (DMSO-d_6 D2O) δ: 3.85 (s, 3H, OCH_3), 7.12 (d, J = 8.88, 2H, Ar-H), 7.41–7.44 (m, 2H, Ar-H of pyridine and CH furan), 7.79 (d, J = 8.84, 2H, Ar-H), 8.30 (s, 1H, NH, D_2O exchangeable), 8.38 (dt, J = 7.88, 1.87, 1H, Ar-H of pyridine), 8.55 (s, 1H, CH pyrimidine), 8.62 (dd, J = 4.76, 1.68, 1H, Ar-H of pyridine), 9.28 (d, J = 1.32, 1H, Ar-H of pyridine), 9.42 (s, 1H, NH, D_2O exchangeable). ^{13}C NMR (DMSO-d_6) δ: 55.85 (—OCH_3), 98.42, 104.48, 115.31, 121.14, 123.40, 126.84, 133.40, 136.02, 148.92, 149.84, 150.51, 154.63, 162.67 (Ar-C*s*), 160.90 (—C═NH), 169.60 (C═O). Anal. Calcd. for $C_{19}H_{15}N_5O_3$ (361.36): C, 63.15; H, 4.18; N, 19.38. Found: C, C, 63.36; H, 4.37; N, 19.61.

4.1.3.1.3. N-(4-Imino-6-(4-methoxyphenyl)furo[2,3-d]pyrimidin-3 (4H)-yl)-4-methoxybenzamide ***(7c)***. Creamy white powder; yield, 60%; m.p., > 300 °C; IR (KBr) $\nu_{max.}$/cm^{-1}: 3406 ($NH_{(s)}$), 3097 (CH aromatic), 2939 (CH aliphatic), 1651 (C═O), 1612 (NH bending), 1500, 1465 (C═C aromatic). ^1H NMR (DMSO-d_6 D2O) δ: 3.84 (s, 3H, OCH_3), 3.86 (s, 3H, OCH_3), 7.02 (d, J = 8.52, 2H, Ar-H), 7.13 (d, J = 8.60, 2H, Ar-H), 7.47 (s, 1H, CH furan), 7.80 (d, J = 8.60, 2H, Ar-H), 8.05 (d, J = 8.56, 2H, Ar-H), 8.67 (s, 1H, CH pyrimidine), 9.62 (s, 1H, NH, D_2O exchangeable), 9.74 (s, 1H, NH, D_2O exchangeable). ^{13}C NMR (DMSO-d_6) δ: 55.79, 55.90 (2 OCH_3), 98.69, 104.73, 113.52, 115.37, 121.03, 126.92, 130.44, 149.70, 151.44, 154.92, 161.30, 161.90 (Ar-C*s*), 161.01 (—C═NH), 169.40 (C═O). Anal. Calcd. for $C_{21}H_{18}N_4O_4$ (390.40): C, 64.61; H, 4.65; N, 14.35. Found: C, 64.87; H, 4.81; N, 14.60.

4.1.3.2. General procedures for preparation of compounds ***7d-f***. In absolute ethanol (5 ml) or dry dimethyl formamide (DMF) (5 ml); ethyl-N-(3-cyano-5-phenylfuran-2-yl)formimidate **3b** (2.40 g, 10 mmol) and the appropriate acid hydrazide derivative **5a-c** (10 mmol) were heated under reflux for 1 h. The reaction mixture was cooled to 0 °C. The obtained solid was filtered, washed with hexane, and left to dry to give **7d-f**, respectively.

4.1.3.2.1. N-(4-Imino-6-phenylfuro[2,3-d]pyrimidin-3(4H)-yl)benzamide ***(7d)***. Creamy white powder; yield, 73%; m.p., > 300 °C; IR (KBr) $\nu_{max.}$/cm^{-1}: 3390 ($NH_{(s)}$), 3132 (CH aromatic), 1662 (C═O), 1585 (NH bending), 1550, 1492 (C═C aromatic). ^1H NMR (DMSO-d_6 D2O) δ: 7.34–7.45 (m, 3H, Ar-H and CH furan), 7.48 (t, J = 7.40, 1H, Ar-H), 7.56–7.61 (m, 3H, Ar-H), 7.85 (d, J = 7.36, 2H, Ar-H), 8.13 (d, J = 7.52, 2H, Ar-H), 8.25 (s, 1H, NH, D_2O exchangeable), 8.55 (s, 1H, CH pyrimidine), 9.48 (s, 1H, NH, D_2O exchangeable). ^{13}C NMR (DMSO-d_6) δ: 100.48, 104.21, 125.07, 127.83, 128.53, 128.66, 129.86, 130.17, 138.40, 149.90, 150.74, 154.08 (Ar-C*s*), 161.42 (—C═NH), 170.71 (C═O). Anal. Calcd. for $C_{19}H_{14}N_4O_2$ (330.35): C, 69.08; H, 4.27; N, 16.96. Found: C, 69.24; H, 4.35; N, 17.13.

4.1.3.2.2. N-(4-Imino-6-phenylfuro[2,3-d]pyrimidin-3(4H)-yl)-3-pyridinamide ***(7e)***. Creamy white powder; yield, 62%; m.p., > 300 °C; IR (KBr) $\nu_{max.}$/cm^{-1}: 3321 ($NH_{(s)}$), 3043 (CH aromatic), 1678 (C═O), 1589 (NH bending), 1550, 1519, 1489 (C═C aromatic). ^1H NMR (DMSO-d_6 D2O) δ: 7.42–7.52 (m, 2H, Ar-H of pyridine and Ar-H), 7.57 (t, J = 7.72, 3H, Ar-H and CH furan), 7.85 (d, J = 7.40, 2H, Ar-H), 8.37 (d, J = 6.08, 1H, Ar-H of pyridine), 8.39 (s, 1H, NH, D_2O exchangeable), 8.59 (s, 1H, CH pyrimidine), 8.62 (dd, J = 4.74, 1.58, 1H, Ar-H of pyridine), 9.29 (s, 1H, Ar-H of pyridine), 9.51 (s, 1H, NH, D_2O exchangeable). ^{13}C NMR (DMSO-d_6) δ: 100.46, 104.29, 123.28, 125.08, 128.61, 129.86, 130.21, 133.58, 135.84, 149.69, 149.97, 150.68, 150.71, 154.17 (Ar-C*s*), 161.46 (—C═NH), 169.30 (C═O). Ms, *m/z* (%): 331 (M^+, 17.28). Anal. Calcd. for $C_{18}H_{13}N_5O_2$ (331.34): C, 65.25; H, 3.95; N, 21.14. Found: C, 65.03; H, 4.11; N, 21.26.

4.1.3.2.3. N-(4-Imino-6-phenylfuro[2,3-d]pyrimidin-3(4H)-yl)-4-methoxybenzamide ***(7f)***. White powder; yield, 52%; m.p., > 300 °C; IR (KBr) $\nu_{max.}$/cm^{-1}: 3379 ($NH_{(s)}$), 3093 (CH aromatic), 2997 (CH aliphatic), 1658 (C═O), 1608 (NH bending), 1597, 1562, 1531 (C═C aromatic). ^1H NMR (DMSO-d_6 D2O) δ: 3.81 (s, 3H, OCH_3), 6.93 (d, J = 8.72, 2H, Ar-H), 7.50 (t, J = 7.34, 1H, Ar-H), 7.58 (t, J = 7.76, 3H, Ar-H and CH furan), 7.85 (d, J = 7.36, 2H, Ar-H), 8.06 (d, J = 8.72, 2H, Ar-H), 8.21 (s, 1H, NH, D_2O exchangeable), 8.52 (s, 1H, CH pyrimidine), 9.44 (s, 1H, NH, D_2O exchangeable). ^{13}C NMR (DMSO-d_6) δ: 55.61 (—OCH_3), 100.50, 104.19, 113.07, 125.05, 128.68, 129.85, 130.08, 130.14, 150.02, 150.78, 154.01, 161.33 (Ar-C*s*), 160.96 (—C═NH), 170.02 (C═O). Anal. Calcd. for $C_{20}H_{16}N_4O_3$ (360.37): C, 66.66; H, 4.48; N, 15.55. Found: C, 66.59; H, 4.67; N, 15.72.

4.1.4. General procedures for preparation of compounds ***8a-f***

Method (1): Compounds **7a-f** (10 mmol) in bromobenzene (10 ml) were heated under reflux for 24 h, then cooled. The obtained solid was filtered, washed with ethanol, left to dry and crystallized from dioxane to give **8a-f**, respectively.

Method (2): Ethyl-N-(3-cyano-5-arylfuran-2-yl)formimidate **3a** or **b** (10 mmol) and acid hydrazide derivative **5a-c** (10 mmol) in bromobenzene (10 ml) were heated under reflux for 24 h. The reaction mixture was left to cool at room temperature. The obtained solid was filtered, washed with ethanol, dried and recrystallized from dioxane to give **8a-f**, respectively.

4.1.4.1. 8-(4-Methoxyphenyl)-2-phenylfuro[3,2-e][1,2,4]triazolo[1,5-c] pyrimidine ***(8a)***. Shiny buff powder; yield, 71%; m.p., 245–246 °C; IR (KBr) $\nu_{max.}$/cm^{-1}: 3082, 3059 (CH aromatic), 2943 (CH aliphatic), 1643 (C═N), 1535, 1500 (C═C aromatic). ^1H NMR (DMSO-d_6 D2O) δ: 3.84 (s, 3H, OCH_3), 7.10 (d, J = 8.80, 2H, Ar-H), 7.59–7.60 (m, 2H, Ar-H), 7.80 (s, 1H, CH furan), 7.94 (d, J = 8.72, 3H, Ar-H), 8.27–8.29 (m, 1H, Ar-H), 8.70 (s, 1H, Ar-H), 9.66 (s, 1H, CH pyrimidine). ^{13}C NMR (DMSO-d_6) δ: 55.85 (—OCH_3), 98.82, 108.21, 115.17, 121.63, 126.96, 127.62, 129.55, 130.31, 131.31, 137.41, 148.73, 155.52, 156.07, 157.29, 160.84 (Ar-C*s*). Ms, *m/z* (%): 342 (M^+, 41.89). Anal. Calcd. for $C_{20}H_{14}N_4O_2$ (342.36): C, 70.17; H, 4.12; N, 16.37. Found: C, 69.88; H, 4.34; N, 16.28.

4.1.4.2. 8-(4-Methoxyphenyl)-2-(pyridin-3-yl)furo[3,2-e][1,2,4]triazolo [1,5-c]pyrimidine ***(8b)***. Shiny buff powder; yield, 65%; m.p., > 300 °C; IR (KBr) $\nu_{max.}$/cm^{-1}: 3097 (CH aromatic), 2970 (CH aliphatic), 1643 (C═N), 1539, 1500 (C═C aromatic). ^1H NMR (DMSO-d_6 D2O) δ: 3.86 (s, 3H, OCH_3), 7.17 (d, J = 7.12, 2H, Ar-H), 7.57–7.59 (m, 1H, Ar-H), 7.91 (s, 1H, CH furan), 7.98 (d, J = 8.24, 2H, Ar-H), 8.62–8.80 (m, 2H, Ar-H), 9.44 (s, 1H, Ar-H), 9.73 (s, 1H, CH pyrimidine). ^{13}C NMR (DMSO-d_6) δ: 55.90 (—OCH_3), 105.30, 115.78, 116.95, 122.60, 124.77, 127.43, 132.92, 135.75, 141.07, 147.56, 154.71, 155.54, 160.37 (Ar-C*s*). Anal. Calcd. for $C_{19}H_{13}N_5O_2$ (343.35): C, 66.47; H, 3.82; N, 20.40. Found: C, 66.39; H, 4.01; N, 20.57.

4.1.4.3. 2,8-bis(4-Methoxyphenyl)furo[3,2-e][1,2,4]triazolo[1,5-c]pyrimidine ***(8c)***. Shiny light brown powder; yield, 64%; m.p., > 300 °C; IR (KBr) $\nu_{max.}$/cm^{-1}: 3093 (CH aromatic), 2943 (CH aliphatic), 1643 (C═N), 1581, 1500 (C═C aromatic). ^1H NMR (DMSO-d_6 D2O) δ: 3.86 (s, 3H, OCH_3), 3.87 (s, 3H, OCH_3), 7.05–7.15 (m, 4H, Ar-H), 7.96–8.23 (m, 5H, Ar-H and CH furan), 9.62 (s, 1H, CH pyrimidine). ^{13}C NMR (DMSO-d_6) δ: 55.90 (2 OCH_3), 105.14, 114.29, 115.78, 122.60, 124.77, 131.11, 131.76, 141.40, 148.55, 152.21, 159.70, 160.53 (Ar-C*s*). Anal. Calcd. for $C_{21}H_{16}N_4O_3$ (372.38): C, 67.73; H, 4.33; N, 15.05. Found: C, C, 67.91; H, 4.62; N, 15.49.

*4.1.4.4. 2,8-Diphenylfuro[3,2-e][1,2,4]triazolo[1,5-c]pyrimidine **(8d)**.* Shiny buff powder; yield, 62%; m.p., > 300 °C; IR (KBr) $\nu_{max.}/cm^{-1}$: 3101, 3066 (CH aromatic), 1647 (C═N), 1539, 1485 (C═C aromatic). ^{1}H NMR (DMSO-d_6 D2O) δ: 7.48–7.59 (m, 6H, Ar-H and CH furan), 8.03 (m, 3H, Ar-H), 8.29 (br s, 2H, Ar-H), 9.69 (s, 1H, CH pyrimidine). ^{13}C NMR (DMSO-d_6) δ: 105.14, 115.62, 124.77, 127.59, 128.77, 129.09, 130.59, 131.92, 132.75, 140.24, 145.56, 154.71, 159.87 (Ar-C*s*). Anal. Calcd. for $C_{19}H_{12}N_4O$ (312.33): C, 73.07; H, 3.87; N, 17.94. Found: C, 72.89; H, 4.04; N, 17.68.

*4.1.4.5. 8-Phenyl-2-(pyridin-3-yl)furo[3,2-e][1,2,4]triazolo[1,5-c]pyrimidine **(8e)**.* Shiny brown powder; yield, 69%; m.p., > 300 °C; IR (KBr) $\nu_{max.}/cm^{-1}$: 3093, 3047 (CH aromatic), 1643 (C═N), 1573, 1539 (C═C aromatic). ^{1}H NMR (DMSO-d_6 D2O) δ: 7.50–7.66 (m, 4H, Ar-H and CH furan), 8.04–8.08 (m, 3H, Ar-H), 8.59 (d, J = 6.64, 1H, Ar-H of pyridine), 8.79 (br s, 1H, Ar-H of pyridine), 9.44 (s, 1H, CH pyrimidine), 9.76 (s, 1H, Ar-H of pyridine). ^{13}C NMR (DMSO-d_6) δ: 105.14, 116.95, 124.27, 125.43, 128.59, 129.26, 130.42, 132.58, 135.58, 142.23, 147.89, 153.55, 154.71, 158.37 (Ar-C*s*). Ms, *m/z* (%): 314 (M^+ + 1, 26.24). Anal. Calcd. for $C_{18}H_{11}N_5O$ (313.32): C, 69.00; H, 3.54; N, 22.35. Found: C, 68.76; H, 3.78; N, 22.14.

*4.1.4.6. 2-(4-Methoxyphenyl)-8-phenylfuro[3,2-e][1,2,4]triazolo[1,5-c]pyrimidine **(8f)**.* Shiny creamy white powder; yield, 64%; m.p., > 300 °C; IR (KBr) $\nu_{max.}/cm^{-1}$: 3089, 3051 (CH aromatic), 2997 (CH aliphatic), 1647 (C═N), 1581, 1527 (C═C aromatic). ^{1}H NMR (DMSO-d_6 D2O) δ: 3.87 (s, 3H, OCH_3), 7.15 (d, J = 8.20, 2H, Ar-H), 7.35–7.58 (m, 4H, Ar-H and CH furan), 8.03 (br s, 2H, Ar-H), 8.22 (d, J = 8.44, 2H, Ar-H), 9.67 (s, 1H, CH pyrimidine). ^{13}C NMR (DMSO-d_6) δ: 57.23 (—OCH_3), 105.30, 112.29, 115.45, 123.43, 125.43, 129.59, 130.59, 143.06, 148.06, 154.38, 155.54, 160.53, 161.86 (Ar-C*s*). Anal. Calcd. for $C_{20}H_{14}N_4O_2$ (342.36): C, 70.17; H, 4.12; N, 16.37. Found: C, 70.39; H, 4.41; N, 16.63.

*4.1.5. 4-Imino-6-phenylfuro[2,3-d]pyrimidin-3(4H)-amine **(9)***

A solution of ***3a*** (2.40 g, 10 mmol) and hydrazine hydrate (99%, 10 ml, 20 mmol) in absolute ethanol (10 ml) was heated under reflux for 8 h. The excess solvent was evaporated to the least amount and the residual solution was cooled to 0 °C overnight for complete precipitation. The obtained solid was filtered, washed with ethanol and left to dry to give ***9***.

Yellowish orange powder; yield, 50%; m.p., 222–223 °C; IR (KBr) $\nu_{max.}/cm^{-1}$: 3309–3201 (NH_2, NH), 3062 (CH aromatic), 1608 (NH bending), 1589, 1562, 1489 (C═C aromatic). ^{1}H NMR (DMSO-d_6 D2O) δ: 4.72 (s, 2H, NH_2, D_2O exchangeable), 7.40 (t, J = 7.36, 1H, Ar-H), 7.51 (t, J = 7.66, 3H, Ar-H and CH furan), 7.80 (d, J = 7.48, 2H, Ar-H), 8.21 (s, 1H, CH pyrimidine), 9.04 (s, 1H, NH, D_2O exchangeable). ^{13}C NMR (DMSO-d_6) δ: 101.24, 124.53, 126.81, 129.04, 129.61, 129.74 (Ar-C*s*), 153.96 (—C═NH). Ms, *m/z* (%): 226 (M^+, 25.22). Anal. Calcd. for $C_{12}H_{10}N_4O$ (226.24): C, 63.71; H, 4.46; N, 24.76. Found: C, 63.88; H, 4.54; N, 24.52.

*4.1.6. General procedure for preparation of compounds **10a-f***

4-Imino-6-phenylfuro[2,3-*d*]pyrimidin-3(4H)-amine **9** (2.26 g, 10 mmol), the appropriate aromatic aldehyde (15 mmol) in absolute ethanol (10 ml) and few drops of glacial acetic acid were heated under reflux for 8 h. The obtained solid was filtered while hot, purified from ethanol and dried to give **10a-f**, respectively.

*4.1.6.1. 3-(Benzylideneamino)-6-phenylfuro[2,3-d]pyrimidin-4(3H)-imine **(10a)**.* Light yellow powder; yield, 60%; m.p., 228–230 °C; IR (KBr) $\nu_{max.}/cm^{-1}$: 3190 (NH), 3039 (CH aromatic), 1605 (NH bending), 1585, 1489 (C═C aromatic). ^{1}H NMR (DMSO-d_6 D2O) δ: 7.43–7.47 (m, 2H, Ar-H), 7.51–7.57 (m, 4H, Ar-H), 7.61 (s, 1H, CH furan), 7.83 (d, J = 7.64, 2H, Ar-H), 7.96 (d, J = 7.72, 2H, Ar-H), 8.27 (s, 1H, CH pyrimidine), 8.40 (s, 1H, HC═N), 11.99 (s, 1H, NH, D_2O exchangeable). ^{13}C NMR (DMSO-d_6) δ: 101.79, 102.63, 125.14, 127.35, 129.39, 129.54, 129.64, 130.16, 134.72, 145.28, 152.04, 153.76 (Ar-C*s*), 156.30 (HC═N—N), 167.62 (—C═NH). Anal. Calcd. for $C_{19}H_{14}N_4O$ (314.35): C, 72.60; H, 4.49; N, 17.82. Found: C, 72.51; H, 4.68; N, 18.05.

*4.1.6.2. 3-((4-Chlorobenzylidene)amino)-6-phenylfuro[2,3-d]pyrimidin-4(3H)-imine **(10b)**.* Yellowish buff powder; yield, 72%; m.p., 295–296 °C; IR (KBr) $\nu_{max.}/cm^{-1}$: 3197 (NH), 3051 (CH aromatic), 1605 (NH bending), 1593, 1562, 1489 (C═C aromatic). ^{1}H NMR (DMSO-d_6 D2O) δ: 7.46 (t, J = 7.36, 1H, Ar-H), 7.53–7.59 (m, 5H, Ar-H and CH furan), 7.85 (d, J = 8.48, 2H, Ar-H), 7.97 (d, J = 7.40, 2H, Ar-H), 8.26 (s, 1H, CH pyrimidine), 8.40 (s, 1H, HC═N), 12.05 (s, 1H, NH, D_2O exchangeable). ^{13}C NMR (DMSO-d_6) δ: 101.72, 102.70, 125.19, 128.98, 129.34, 129.59, 129.61, 130.49, 133.68, 134.49, 143.91, 152.15, 153.73 (Ar-C*s*), 156.22 (HC═N—N), 167.62 (—C═NH). Anal. Calcd. for $C_{19}H_{13}ClN_4O$ (348.79): C, 65.43; H, 3.76; N, 16.06. Found: C, 65.19; H, 4.02; N, 16.28.

*4.1.6.3. 3-((4-Bromobenzylidene)amino)-6-phenylfuro[2,3-d]pyrimidin-4(3H)-imine **(10c)**.* Creamy white powder; yield, 60%; m.p., 291–293 °C; IR (KBr) $\nu_{max.}/cm^{-1}$: 3194 (NH), 3035 (CH aromatic), 1608 (NH bending), 1593, 1558, 1485 (C═C aromatic). ^{1}H NMR (DMSO-d_6 D2O) δ: 7.45 (t, J = 7.34, 1H, Ar-H), 7.55 (t, J = 7.76, 3H, Ar-H and CH furan), 7.70 (d, J = 8.48, 2H, Ar-H), 7.77 (d, J = 8.48, 2H, Ar-H), 7.96 (d, J = 7.44, 2H, Ar-H), 8.23 (s, 1H, CH pyrimidine), 8.40 (s, 1H, HC═N), 12.04 (s, 1H, NH, D_2O exchangeable). ^{13}C NMR (DMSO-d_6) δ: 101.71, 102.71, 123.24, 125.19, 125.45, 129.21, 129.34, 129.61, 130.67, 134.02, 143.98, 152.16, 153.73 (Ar-C*s*), 161.20 (HC═N—N), 167.63 (—C═NH). Anal. Calcd. for $C_{19}H_{13}BrN_4O$ (393.24): C, 58.03; H, 3.33; N, 14.25. Found: C, 58.14; H, 3.50; N, 14.56.

*4.1.6.4. 4-(((4-Imino-6-phenylfuro[2,3-d]pyrimidin-3(4H)-yl)imino)methyl)-N,N-dimethylaniline **(10d)**.* Yellow powder; yield, 57%; m.p., 275–276 °C; IR (KBr) $\nu_{max.}/cm^{-1}$: 3197 (NH), 3055 (CH aromatic), 2978 (CH aliphatic), 1604 (NH bending), 1519, 1489 (C═C aromatic). ^{1}H NMR (DMSO-d_6 D2O) δ: 3.01 (s, 6H, 2 CH_3), 6.83 (d, J = 8.80, 2H, Ar-H), 7.45 (t, J = 7.34, 1H, Ar-H), 7.55 (t, J = 7.66, 2H, Ar-H), 7.59 (s, 1H, CH furan), 7.64 (d, J = 8.76, 2H, Ar-H), 7.94 (d, J = 7.48, 2H, Ar-H), 8.14 (s, 1H, CH pyrimidine), 8.33 (s, 1H, HC═N), 11.71 (s, 1H, NH, D_2O exchangeable). ^{13}C NMR (DMSO-d_6) δ: 31.15 (2 CH_3), 102.20, 112.14, 112.55, 122.12, 124.97, 128.67, 129.36, 129.62, 129.95, 146.15, 151.45, 151.74, 153.79 (Ar-C*s*), 160.27 (HC═N—N), 167.59 (—C═NH). Anal. Calcd. for $C_{21}H_{19}N_5O$ (357.42): C, 70.57; H, 5.36; N, 19.59. Found: C, 70.81; H, 5.49; N, 19.81.

*4.1.6.5. 3-((4-Methoxybenzylidene)amino)-6-phenylfuro[2,3-d]pyrimidin-4(3H)-imine **(10e)**.* Light yellow powder; yield, 67%; m.p., 268–269 °C; IR (KBr) $\nu_{max.}/cm^{-1}$: 3205 (NH), 3055 (CH aromatic), 2970 (CH aliphatic), 1604 (NH bending), 1589, 1512, 1489 (C═C aromatic). ^{1}H NMR (DMSO-d_6 D2O) δ: 3.84 (s, 3H, OCH_3), 7.08 (d, J = 8.68, 2H, Ar-H), 7.45 (t, J = 7.36, 1H, Ar-H), 7.54 (t, J = 7.62, 2H, Ar-H), 7.59 (s, 1H, CH furan), 7.77 (d, J = 8.68, 2H, Ar-H), 7.95 (d, J = 7.44, 2H, Ar-H), 8.21 (s, 1H, CH pyrimidine), 8.36 (s, 1H, HC═N), 11.85 (s, 1H, NH, D_2O exchangeable). ^{13}C NMR (DMSO-d_6) δ: 55.79 (—OCH_3), 101.95, 102.41, 115.04, 125.08, 127.33, 128.97, 129.48, 129.62, 145.22, 151.78, 153.77 (Ar-C*s*), 161.04 (HC═N—N), 167.60 (—C═NH). Ms, *m/z* (%): 344.68 (M^+, 23.47). Anal. Calcd. for $C_{20}H_{16}N_4O_2$ (344.37): C, 69.76; H, 4.68; N, 16.27. Found: C, 69.53; H, 4.89; N, 16.53.

*4.1.6.6. 4-(((4-Imino-6-phenylfuro[2,3-d]pyrimidin-3(4H)-yl)imino)methyl)-2-methoxyphenol **(10f)**.* Yellow powder; yield, 63%; m.p., 287–289 °C; IR (KBr) $\nu_{max.}/cm^{-1}$: 3525 (OH), 3200 (NH), 3062 (CH aromatic), 2993 (CH aliphatic), 1597 (NH bending), 1516, 1435 (C═C aromatic). ^{1}H NMR (DMSO-d_6 D2O) δ: 3.96 (s, 3H, OCH_3), 6.89 (d, J =

8.08, 1H, Ar-H), 7.18 (dd, $J = 8.12, 1.56$, 1H, Ar-H), 7.41–7.45 (m, 2H, Ar-H), 7.53 (t, $J = 7.62$, 2H, Ar-H), 7.62 (s, 1H, CH furan), 7.88 (d, $J = 7.44$, 2H, Ar-H), 8.15 (s, 1H, CH pyrimidine), 8.36 (s, 1H, HC═N), 9.56 (s, 1H, OH, D_2O exchangeable), 11.85 (s, 1H, NH, D_2O exchangeable). ^{13}C NMR (DMSO-d_6) δ: 55.68 (—OCH_3), 102.29, 102.41, 109.41, 116.14, 121.76, 124.84, 126.24, 129.43, 129.49, 129.66, 145.39, 148.52, 149.11, 151.66, 153.79 (Ar-C*s*), 156.36 (HC═N—N), 167.62 (—C═NH). Anal. Calcd. for $C_{20}H_{16}N_4O_3$ (360.37): C, 66.66; H, 4.48; N, 15.55. Found: C, 66.89; H, 4.56; N, 15.78.

4.1.7. General procedure for preparation of compounds ***12a,b***

Equimolar amounts of 4-Imino-6-phenylfuro[2,3-*d*]pyrimidin-3(4H)-amine **9** and the corresponding 4-(amino substituted) benzaldehyde derivative **11a,b** (10 mmol) were heated under reflux conditions in absolute ethanol (10 ml), with or without addition of few drops of glacial acetic acid, for 4 h. The obtained solid was filtered while hot, purified from ethanol and dried to give **12a,b**, respectively.

4.1.7.1. 3-((4-Morpholinobenzylidene)amino)-6-phenylfuro[2,3-d]pyrimidin-4(3H)-imine ***(12a)***. Yellow powder; yield, 68%; m.p., > 300 °C; IR (KBr) $\nu_{max.}/cm^{-1}$: 3194 (NH), 3059 (CH aromatic), 2951, 2889, 2858 (CH aliphatic), 1604 (NH bending), 1589, 1489, 1438 (C═C aromatic). ^1H NMR (DMSO-d_6 D2O) δ: 3.23 (t, $J = 4.48$, 4H, $N(CH_2)_2$ of morpholine), 3.76 (t, $J = 4.48$, 4H, $O(CH_2)_2$ of morpholine), 7.06 (d, $J = 8.60$, 2H, Ar-H), 7.44 (t, $J = 7.32$, 1H, Ar-H), 7.54 (t, $J = 7.62$, 2H, Ar-H), 7.59 (s, 1H, CH furan), 7.68 (d, $J = 8.56$, 2H, Ar-H), 7.93 (d, $J = 7.64$, 2H, Ar-H), 8.16 (s, 1H, CH pyrimidine), 8.35 (s, 1H, HC═N), 11.78 (s, 1H, NH, D_2O exchangeable). ^{13}C NMR (DMSO-d_6) δ: 48.03 ($N(CH_2)_2$ of morpholine), 66.44 ($O(CH_2)_2$ of morpholine), 102.04, 102.33, 115.14, 125.00, 125.07, 128.51, 129.43, 129.48, 129.62, 145.59, 151.62, 152.41, 153.78 (Ar-C*s*), 156.25 (HC═N—N), 167.59 (—C═NH). Ms, *m/z* (%): 399 (M^+, 13.57), 400 (M^++1, 13.13). Anal. Calcd. for $C_{23}H_{21}N_5O_2$ (399.45): C, 69.16; H, 5.30; N, 17.53. Found: C, 69.21; H, 5.48; N, 17.40.

4.1.7.2. 3-((4-(4-Methylpiperazin-1-yl)benzylidene)amino)-6-phenylfuro[2,3-d]pyrimidin-4(3H)-imine ***(12b)***. Yellowish orange powder; yield, 60%; m.p., 280–282 °C; IR (KBr) $\nu_{max.}/cm^{-1}$: 3201 (NH), 3059 (CH aromatic), 2974, 2885, 2835 (CH aliphatic), 1604 (NH bending), 1589, 1516, 1489 (C═C aromatic). ^1H NMR (DMSO-d_6 D2O) δ: 2.24 (s, 3H, CH_3), 2.46 (t, $J = 4.66$, 4H, $N(CH_2)_2$ of *N*-methylpiperazine), 3.27 (t, $J = 4.62$, 4H, $N(CH_2)_2$ of *N*-methylpiperazine), 7.04 (d, $J = 8.72$, 2H, Ar-H), 7.45 (t, $J = 7.32$, 1H, Ar-H), 7.55 (t, $J = 7.60$, 2H, Ar-H), 7.59 (s, 1H, CH furan), 7.65 (d, $J = 8.68$, 2H, Ar-H), 7.93 (d, $J = 7.52$, 2H, Ar-H), 8.15 (s, 1H, CH pyrimidine), 8.34 (s, 1H, HC═N), 11.79 (s, 1H, NH, D_2O exchangeable). ^{13}C NMR (DMSO-d_6) δ: 46.21 (CH_3), 47.66 ($N(CH_2)_2$ of *N*-methylpiperazine), 54.88 ($N(CH_2)_2$ of *N*-methylpiperazine), 102.02, 102.31, 115.28, 124.59, 124.98, 128.51, 129.41, 129.48, 129.62, 145.64, 151.58, 152.29, 153.78 (Ar-C*s*), 156.23 (HC═N—N), 167.59 (—C═NH). Anal. Calcd. for $C_{24}H_{24}N_6O$ (412.50): C, 69.88; H, 5.86; N, 20.37. Found: C, 69.72; H, 6.02; N, 20.49.

4.1.8. General procedure for synthesis of compounds ***14a-d***

4-Hydroxy-3-methoxy-5-(substituted-1-ylmethyl)benzaldehyde derivatives **13a-d** (10 mmol) and 4-Imino-6-phenylfuro[2,3-*d*]pyrimidin-3(4H)-amine **9** (2.26 g, 10 mmol) with few drops of glacial acetic acid were refluxed for 4 h in absolute ethanol (10 ml). The obtained solid was filtered while hot, purified from ethanol and left to dry to give **14a-d**, respectively.

4.1.8.1. 4-(((4-Imino-6-phenylfuro[2,3-d]pyrimidin-3(4H)-yl)imino)methyl)-2-methoxy-6-(pyrrolidin-1-ylmethyl)phenol ***(14a)***. Shiny yellow powder; yield, 55%; m.p., 210–211 °C; IR (KBr) $\nu_{max.}/cm^{-1}$: 3394 (OH), 3197 (NH), 3062 (CH aromatic), 2966 (CH aliphatic), 1597 (NH bending), 1554, 1500 (C═C aromatic). ^1H NMR (DMSO-d_6 D2O) δ: 1.77 (br s, 4H, 2 CH_2 of pyrrolidine), 2.60 (br s, 4H, 2 $N(CH_2)_2$ of pyrrolidine), 3.83 (s, 2H, N-CH_2), 3.94 (s, 3H, OCH_3), 7.11 (s, 1H, Ar-H), 7.34 (s, 1H, Ar-H), 7.43 (t, $J = 7.38$, 1H, Ar-H), 7.53 (t, $J = 7.58$, 2H, Ar-H), 7.62 (s, 1H, CH furan), 7.85 (d, $J = 7.32$, 2H, Ar-H), 8.13 (s, 1H, CH pyrimidine), 8.36 (s, 1H, HC═N), 11.85 (s, 1H, NH, D_2O exchangeable). ^{13}C NMR (DMSO-d_6) δ: 23.68 (2 CH_2 of pyrrolidine), 53.56 ($N(CH_2)_2$ of pyrrolidine), 55.77 (—OCH_3), 56.44 (—N-CH_2), 102.42, 108.14, 121.31, 124.15, 124.74, 125.23, 129.44, 129.51, 129.65, 145.33, 148.29, 148.77, 151.61, 153.81 (Ar-C*s*), 156.38 (HC═N—N), 167.63 (—C═NH). Anal. Calcd. for $C_{25}H_{25}N_5O_3$ (443.51): C, 67.70; H, 5.68; N, 15.79. Found: C, 67.52; H, 5.85; N, 16.03.

4.1.8.2. 4-(((4-Imino-6-phenylfuro[2,3-d]pyrimidin-3(4H)-yl)imino)methyl)-2-methoxy-6-(piperidin-1-ylmethyl)phenol ***(14b)***. Yellowish buff powder; yield, 53%; m.p., 233–234 °C; IR (KBr) $\nu_{max.}/cm^{-1}$: 3417 (OH), 3205 (NH), 3062 (CH aromatic), 2935, 2854, 2800 (CH aliphatic), 1600 (NH bending), 1492 (C═C aromatic). ^1H NMR (DMSO-d_6 D2O) δ: 1.45–1.46 (m, 2H, CH_2 of piperidine), 1.55–1.57 (m, 4H, 2 CH_2 of piperidine), 2.48–2.51 (m, 4H, $N(CH_2)_2$ of piperidine), 3.71 (s, 2H, N-CH_2), 3.94 (s, 3H, OCH_3), 7.06 (s, 1H, Ar-H), 7.35 (s, 1H, Ar-H), 7.44 (t, $J = 7.38$, 1H, Ar-H), 7.54 (t, $J = 7.60$, 2H, Ar-H), 7.63 (s, 1H, CH furan), 7.86 (d, $J = 7.48$, 2H, Ar-H), 8.12 (s, 1H, CH pyrimidine), 8.36 (s, 1H, HC═N), 11.86 (s, 1H, NH, D_2O exchangeable). ^{13}C NMR (DMSO-d_6) δ: 24.01 (CH_2 of piperidine), 25.89 (2 CH_2 of piperidine), 53.69 ($N(CH_2)_2$ of piperidine), 55.68 (—OCH_3), 60.08 (—N-CH_2), 102.10, 102.40, 108.08, 121.59, 122.95, 124.74, 125.23, 129.44, 129.49, 129.69, 145.40, 148.31, 149.22, 151.66, 153.80 (Ar-C*s*), 156.38 (HC═N—N), 167.58 (—C═NH). Anal. Calcd. for $C_{26}H_{27}N_5O_3$ (457.53): C, 68.25; H, 5.95; N, 15.31. Found: C, 68.46; H, 6.12; N, 15.53.

4.1.8.3. 4-(((4-Imino-6-phenylfuro[2,3-d]pyrimidin-3(4H)-yl)imino)methyl)-2-methoxy-6-(morpholinomethyl)phenol ***(14c)***. Buff powder; yield, 73%; m.p., 230–231 °C; IR (KBr) $\nu_{max.}/cm^{-1}$: 3410 (OH), 3201 (NH), 3059 (CH aromatic), 2927, 2873, 2827 (CH aliphatic), 1612 (NH bending), 1492 (C═C aromatic). ^1H NMR (DMSO-d_6 D2O) δ: 2.48–2.50 (m, 4H, $N(CH_2)_2$ of morpholine), 3.61 (t, $J = 4.06$, 4H, $O(CH_2)_2$ of morpholine), 3.68 (s, 2H, N-CH_2), 3.96 (s, 3H, OCH_3), 7.15 (s, 1H, Ar-H), 7.36 (s, 1H, Ar-H), 7.44 (t, $J = 7.36$, 1H, Ar-H), 7.53 (t, $J = 7.58$, 2H, Ar-H), 7.63 (s, 1H, CH furan), 7.86 (d, $J = 7.36$, 2H, Ar-H), 8.14 (s, 1H, CH pyrimidine), 8.36 (s, 1H, HC═N), 11.87 (s, 1H, NH, D_2O exchangeable). ^{13}C NMR (DMSO-d_6) δ: 53.25 ($N(CH_2)_2$ of morpholine), 55.81 (—OCH_3), 58.61 (—N—CH_2), 66.61 ($O(CH_2)_2$ of morpholine), 102.25, 102.42, 108.14, 122.06, 123.17, 124.75, 125.52, 129.46, 129.67, 145.31, 148.19, 148.31, 151.66, 153.80 (Ar-C*s*), 156.35 (HC═N—N), 167.61 (—C═NH). Anal. Calcd. for $C_{25}H_{25}N_5O_4$ (459.51): C, 65.35; H, 5.48; N, 15.24. Found: C, 65.54; H, 5.62; N, 15.56.

4.1.8.4. 4-(((4-Imino-6-phenylfuro[2,3-d]pyrimidin-3(4H)-yl)imino)methyl)-2-methoxy-6-((4-methylpiperazin-1-yl)methyl)phenol ***(14d)***. Yellow powder; yield, 67%; m.p., 227–229 °C; IR (KBr) $\nu_{max.}/cm^{-1}$: 3425 (OH), 3201 (NH), 3055 (CH aromatic), 2943, 2877, 2808 (CH aliphatic), 1597 (NH bending), 1539, 1492 (C═C aromatic). ^1H NMR (DMSO-d_6 D2O) δ: 2.16 (s, 3H, CH_3), 2.35–2.51 (m, 8H, 2 $N(CH_2)_2$ of *N*-methylpiperazine), 3.71 (s, 2H, N-CH_2), 3.94 (s, 3H, OCH_3), 7.09 (s, 1H, Ar-H), 7.35 (s, 1H, Ar-H), 7.44 (t, $J = 7.34$, 1H, Ar-H), 7.54 (t, $J = 7.62$, 2H, Ar-H), 7.63 (s, 1H, CH furan), 7.86 (d, $J = 7.48$, 2H, Ar-H), 8.13 (s, 1H, CH pyrimidine), 8.36 (s, 1H, HC═N), 11.87 (s, 1H, NH, D_2O exchangeable). ^{13}C NMR (DMSO-d_6) δ: 46.07 (CH_3), 52.57 ($N(CH_2)_2$ of *N*-methylpiperazine), 55.05 ($N(CH_2)_2$ of *N*-methylpiperazine), 55.76 (—OCH_3), 58.84 (—N—CH_2), 102.43, 108.14, 121.82, 123.11, 124.79, 125.44, 129.45, 129.50, 129.67, 145.29, 148.32, 148.63, 151.65, 153.82 (Ar-C*s*), 156.38 (HC═N—N), 167.64 (—C═NH). Ms, *m/z* (%): 472 (M^+, 12.91). Anal. Calcd. for $C_{26}H_{28}N_6O_3$ (472.55): C, 66.09; H, 5.97; N, 17.78. Found: C, 66.23; H, 6.16; N, 17.95.

4.2. Biological evaluation

4.2.1. VEGFR-2 inhibitory activity and structure activity relationship

VEGFR-2 kinase activity was evaluated by means of VEGFR2 (KDR) Kinase Assay Kit (San Diego, CA, USA) according to manufacturer's instructions. The VEGFR2 Kinase Assay Kit can be used to measure VEGFR-2 kinase activity for screening and profiling applications utilizing Kinase-Glo Max as a detection reagent. The VEGFR2 Kinase Assay Kit comes in a convenient 96-well format. Briefly, 25 µl of the master mixture were added to each well. This mixture was prepared as 6 µl 5x Kinase Buffer 1, 1 µl ATP (500 µM), 1 µl 50x PTK substrate and 17 µl water. Then, to each well labeled as test inhibitor 5 µl of inhibitor solution were added. For the positive control and blank wells, 5 µl of the same solution without inhibitor were added. 3 ml of 1x Kinase Buffer 1 were prepared by mixing 600 µl of 5x Kinase Buffer 1 with 2400 µl water. Then, 20 µl of 1x Kinase Buffer 1 were added to the blank wells. The amount of VEGFR-2 required for the assay was calculated and diluted to 1 ng/µl with 1x Kinase Buffer 1. After that, 20 µl of the diluted VEGFR-2 enzyme were added to the wells of positive control and test inhibitor, then the plate was incubated at 30 °C for 45 min. After the 45 min, 50 µl of Kinase-Glo Max reagent were added to each well. The plate was covered with aluminum foil and incubated at room temperature for 15 min. Finally, the luminescence was measured using the microplate reader. The concentration of the test solutions which inhibited the activity of the enzyme by 50% was determined (IC_{50}) by plotting the percentage inhibition of each compound concentration against the log of the concentration of the respective compound and the IC_{50} value for each plot was obtained using computer-assisted non-linear regression analyses. Data presented are the results of at least two independent experiments done in triplicate. The results of these studies are presented as mean IC_{50} (nM) ± standard deviation (SD)[64,65].

4.2.2. NCI-60 human tumor cell lines screen

Fifteen compounds were selected for NCI-60 Human Tumor Cell Lines Screen by the Developmental Therapeutics Program (DTP) at the National Cancer Institute (NCI), Maryland, USA. The compounds were supplied as dry powder and tested against the full 60 cell lines panel representing leukemia, NSCLC, colon, CNS, melanoma, ovarian, renal, prostate and breast cancers at a single dose of 10 µM solution in dimethyl sulfoxide (DMSO) using Sulforhodamine B assay. Briefly, cells were seeded in 96 well plates at an appropriate density and incubated for 1 day. After 1 day, some of the plates were processed to determine the density at time zero. To the remaining plates, compounds were added at a concentration of 10 µM. Plates are incubated for further 2 days, then fixed and stained with sulphorhodamine B. Growth inhibition was calculated relative to cells without drug treatment and the time zero control. The use of a time zero control allows the determination of cell kill as well as net growth inhibition.

4.2.3. Antiproliferative activity against HUVECs

Antiproliferative activity of **8a-c** and **10c** in HUVECs was measured using *in vitro* MTT based toxicology assay kit (catalog no. M-5655, M-8910) (Sigma Aldrich), spectrophotometrically, according to the manufacturer's protocol. Cells were plated (cells density 1.2–1.8 × 10,000 cells/well) in a volume of 100 µl complete growth medium and 100 µl of the tested compound per well in a 96-well plate for 48 h before the MTT assay. The cultures were removed from incubator into laminar flow hood. Each vial of 3-[4,5-dimethylthiazol-2-yl]-2,5-diphenyl tetrazolium bromide (MTT) [M-5655] were reconstituted with 3 ml of medium or balanced salt solution without phenol red and serum. Then, the reconstituted MTT was added in an amount equal to 10% of the culture medium volume and the cultures were returned to incubator for 2–4 h. The cultures were removed from incubator and the resulting formazan crystals were dissolved by gentle mixing with an amount of MTT solubilization solution [M-8910] equal to the original culture medium volume. Finally, the absorbance was measured spectrophotometrically at a wavelength of 570 nm. The background absorbance of multiwell plates was measured at 690 nm and subtracted from the 570 nm measurement. To determine the IC_{50} value for each compound, the percentage viability of each compound concentration was plotted against the log of the concentration of the respective compound and the IC_{50} value for each plot was obtained using computer-assisted non-linear regression analyses. Data presented are the results of at least two independent experiments done in triplicate. The results of these studies are presented as mean IC_{50} (µM) ± standard deviation (SD)[66].

4.2.4. Cell cycle analysis and apoptotic effect on HUVECs

The effect of compounds **8a-c** and **10c** on the cell cycle profile of HUVECs was determined using Annexin V-FITC Apoptosis Detection Kit (Bio Vision) according to the manufacturer's procedures. Briefly, HUVECs were cultured and incubated with each of the tested compounds for 48 h. Then, the cells were collected by centrifugation and resuspended in 500 µl of 1X binding buffer. 5 µl of Annexin V-FITC was added and 5 µl of propidium iodide (PI 50 mg/ml, optional.). the cells were incubated at room temperature for 5 min in the dark. Annexin V-FITC binding was analyzed by flow cytometry (Ex = 488 nm; Em = 530 nm) using FITC signal detector and PI staining was analyzed by the phycoerythrin emission signal detector[67].

4.2.5. Cell invasion and migration assay

Two different methods were used to assess the inhibitory effect of **8a-c** and **10c** on invasion and migration of HUVECs. A) Trans well membrane assay, EZCell™ Cell Invasion Assay (Basement Membrane), 8 µm (Bio Vision), was used according to the manufacturer's assay protocol. The desired wells of the top chamber were coated with 40 µl of basement membrane solution. The plate was incubated at 37 °C in an incubator for 1 h to allow the basement membrane solution to gel. Then, cells of interest were cultured in desired media and culture conditions. Prior to the assay, cells were starved for 18–24 h in a serum-free media (0.5% serum can be used, if needed). After starvation, the cells were harvested and centrifuged for 5 min. to pellet cells. The cells were resuspended in wash buffer and the number of cells were counted using hemocytometer or automated cell counter. The cells were resuspended at 1×10^6 cells/ml in a serum-free media. After that, the cell invasion chamber was disassembled and the plate cover and the top chamber were carefully removed, under sterile conditions. In the bottom chamber, for each well 200 µl of medium containing desired chemoattractant were added except for control well(s), the chemoattractant should be omitted. While, for positive control, 20 µl of control invasion inducer to 180 µl of medium were added in the bottom chamber. The top and bottom chambers were reassembled while ensuring no air bubbles were trapped between them. On the other hand, 50 µl (~50,000 cells) of cell suspension were added to each well of the top chamber. The desired stimulator or inhibitor was added to the top well, and gently mix. The volume was made up to 100 µl with media. The plate cover was carefully replaced, and the cell invasion chamber was incubated at 37 °C in CO_2 incubator for 2–48 h. After incubation period, the plate cover was removed and from the top chamber the media was aspirated, and the cells were removed using a cotton swab. Then, the top chamber was removed, the plate cover was placed on the top of the bottom chamber and the plate was centrifuged for 5 min. at room temperature. The media was aspirated carefully from the bottom chamber, and the chamber was washed with 200 µl of wash buffer. A mixture of 100 µl of cell invasion dye in 1 ml of cell dissociation solution were prepared, from which 100 µl were added to each well of the bottom chamber. The cell invasion chamber was reassembled by placing the top chamber into the bottom chamber and incubated at 37 °C in CO_2 incubator for 60 min. Finally, the top chamber and the bottom well were read at Em/Ex = 530/590 nm. The number of cells invaded was calculated using the equation of the straight line obtained from standard curve[54].

B) Wound healing assay, Cell Biolabs CytoSelect™ 24-Well Wound Healing Assay Kit, was used as the manufacturer's procedures. The 24-

well plate with CytoSelect™ Wound Healing inserts was left to warm up at room temperature for 10 min. The desired number of inserts was oriented in the plate wells with their "wound field" aligned in the same direction and had firm contact with the bottom of the plate well. A cell suspension containing 0.5–1.0 × 106 cells/ml in media containing 10% fetal bovine serum (FBS) was prepared, from which 500 µl were added per well. The cells were incubated in a cell culture incubator overnight or until a monolayer formed. The insert was removed carefully from the well to begin the wound healing assay. Then, the media was aspirated from the wells and the wells was washed with media to remove dead cells and debris. The media with FBS and/or compounds was added to continue cell culture and wound healing process. The cells were incubated in a cell culture incubator for 72 h. The wound closure was monitored with a light microscope or imaging software and the percent closure or the migration rate of the cells into the wound field was measured. Wound healing results can be visualized with phase contrast, DAPI (4′,6-diamidino-2-phenylindole) fluorescence labeling, or cell staining. Data presented are the results of at least two independent experiments done in triplicate. The results of these studies are presented as % closure ± standard deviation (SD)[55–57].

4.3. Molecular docking and drug-likeness study

The parameters of Amber10:EHT forcefield in MOE was selected for potential setup. Amber10:EHT forcefield uses the following parameters: AMBER parameters for proteins and nucleic acids (ff10), EHT parameters for small molecules, AM1-BCC charges are expected for small molecules and Group II ion and Group VIII parameters from OPLS-AA. The co-crystal structures of VEGFR-2 in complex with sunitinib **I** (PDB: 4AGD)[58], sorafenib **III** (PDB: 3WZE)[59] and **VII** (PDB:3VHK)[23], respectively were downloaded from Protein Data Bank available at http://www.rcsb.org/pdb in PDB format. The protein–ligand complexes were prepared by removal of water molecules of crystallization that were not involved in the binding. Protonation of the co-crystal structure was performed, where hydrogen atoms were added at their standard geometry, the partial charges were computed, and the system was optimized using "QuickPrep" preparation protocol in MOE. Isolation of the active site and recognition of the involved amino acids for each co-crystal structure was carried out using "Site View" tool. The 2D interaction diagrams of the co-crystallized ligands, sunitinib **I**, sorafenib **III** and **VII** with VEGFR-2 were isolated using "Ligand Interactions" tool in MOE. The compounds were built using ChemBioDraw Ultra 19.0 and their SMILES were copied to MOE. 3D Protonation of the compounds was carried out using the precise mode in "Protonate" tool and the most prevalent ionized form was selected for subsequent steps. Energy minimization of the structures using 10:EHT forcefield and a gradient of 0.05 was applied using "Energy Minimize" tool. The partial charges were automatically calculated for each molecule. Conformational analysis was run using the default settings for systematic search. The least energy conformer of each molecule was saved to another data base to be docked into the catalytic domain of VEGFR-2 in the three co-crystal structures. Docking of the least energy conformers was performed by definition of the receptor atoms as (receptor) and site of placement was defined as (ligand atoms). The database containing the least energy conformers of the target compounds was used as the input for the docking procedure. Placement method was adjusted to (triangle matcher). Rescoring method was adjusted to (London dG). Finally, the docking poses were examined for protein ligand-interactions and the docking scores were recorded.

The physicochemical properties and drug-likeness profiles of compounds **8a-c** and **10c** were predicted using the free online server SwissADME (http://www.swissadme.ch/index.php). The SMILES of the compounds were inserted directly on the webpage followed by running the prediction process. A whole set of the different physical properties, pharmacokinetic parameters and drug-likeness parameters were obtained online and explained[60].

Declaration of Competing Interest

The authors declare that they have no known competing financial interests or personal relationships that could have appeared to influence the work reported in this paper.

Acknowledgement

The authors are grateful for the members of the Developmental Therapeutics Program (DTP) at the National cancer Institute (NCI), Maryland, USA for performing the NCI-60 Human Tumor Cell Lines Screen. We are greatly thankful to Dr. Tamer Elwaie for critical reading of the manuscript and his valuable suggestions.

Appendix A. Supplementary material

Supplementary data to this article can be found online at https://doi.org/10.1016/j.bioorg.2021.105336.

References

[1] L.A. Torre, R.L. Siegel, E.M. Ward, A. Jemal, Global cancer incidence and mortality rates and trends - An update, Cancer Epidemiol. Biomarkers Prev. 25 (1) (2016) 16–27, https://doi.org/10.1158/1055-9965.EPI-15-0578.
[2] M.M. Fidler, S. Gupta, I. Soerjomataram, J. Ferlay, E. Steliarova-Foucher, F. Bray, Cancer incidence and mortality among young adults aged 20–39 years worldwide in 2012: a population-based study, Lancet Oncol. 18 (12) (2017) 1579–1589, https://doi.org/10.1016/S1470-2045(17)30677-0.
[3] J. Ferlay, I. Soerjomataram, R. Dikshit, S. Eser, C. Mathers, M. Rebelo, D.M. Parkin, D. Forman, F. Bray, Cancer incidence and mortality worldwide: Sources, methods and major patterns in GLOBOCAN 2012, Int. J. Cancer. 136 (5) (2015) E359–E386, https://doi.org/10.1002/ijc.29210.
[4] H. Sung, J. Ferlay, R.L. Siegel, M. Laversanne, I. Soerjomataram, A. Jemal, F. Bray, Global cancer statistics 2020: GLOBOCAN estimates of incidence and mortality worldwide for 36 cancers in 185 Countries, CA. Cancer J. Clin. 71 (3) (2021) 209–249, https://doi.org/10.3322/caac.21660.
[5] N. Nishida, H. Yano, T. Nishida, T. Kamura, M. Kojiro, Angiogenesis in cancer, Vasc. Health Risk Manag. 2 (3) (2006) 213–219, https://doi.org/10.2147/vhrm.2006.2.issue-310.2147/vhrm.2006.2.3.213.
[6] J.-J. Liu, T.-S. Huang, W.-F. Cheng, F.-J. Lu, Baicalein and baicalin are potent inhibitors of angiogenesis: Inhibition of endothelial cell proliferation, migration and differentiation, Int. J. Cancer. 106 (4) (2003) 559–565, https://doi.org/10.1002/(ISSN)1097-021510.1002/ijc.v106:410.1002/ijc.11267.
[7] M. Shibuya, Vegf-vegfr signals in health and disease, Biomol. Ther. 22 (1) (2014) 1–9, https://doi.org/10.4062/biomolther.2013.113.
[8] M. Shibuya, Vascular endothelial growth factor (VEGF) and its receptor (VEGFR) signaling in angiogenesis: A crucial target for anti- and pro-angiogenic therapies, Genes and Cancer. 2 (12) (2011) 1097–1105, https://doi.org/10.1177/1947601911423031.
[9] K.M. Dameron, O. V. Volpert, M.A. Tainsky, N. Bouck, Control of angiogenesis in fibroblasts by p53 regulation of thrombospondin-1, Science (80-.). 265 (1994) 1582–1584. https://doi.org/10.1126/science.7521539.
[10] C.S. Abhinand, R. Raju, S.J. Soumya, P.S. Arya, P.R. Sudhakaran, VEGF-A/VEGFR2 signaling network in endothelial cells relevant to angiogenesis, J. Cell Commun. Signal. 10 (4) (2016) 347–354, https://doi.org/10.1007/s12079-016-0352-8.
[11] W.A. Spannuth, A.M. Nick, N.B. Jennings, G.N. Armaiz-Pena, L.S. Mangala, C. G. Danes, Y.G. Lin, W.M. Merritt, P.H. Thaker, A.A. Kamat, L.Y. Han, J.R. Tonra, R. L. Coleman, L.M. Ellis, A.K. Sood, Functional significance of VEGFR-2 on ovarian cancer cells, Int. J. Cancer. 124 (5) (2009) 1045–1053, https://doi.org/10.1002/ijc.v124:510.1002/ijc.24028.
[12] N. Ferrara, Vascular endothelial growth factor: Basic science and clinical progress, Endocr. Rev. 25 (2004) 581–611, https://doi.org/10.1210/er.2003-0027.
[13] M. Kim, H.J. Park, J.W. Seol, J.Y. Jang, Y.S. Cho, K.R. Kim, Y. Choi, J.P. Lydon, F. J. Demayo, M. Shibuya, N. Ferrara, H.K. Sung, A. Nagy, K. Alitalo, G.Y. Koh, VEGF-A regulated by progesterone governs uterine angiogenesis and vascular remodelling during pregnancy, EMBO Mol. Med. 5 (2013) 1415–1430, https://doi.org/10.1002/emmm.201302618.
[14] S.K. Mukherji, Bevacizumab (avastin), Am. J. Neuroradiol. 31 (2) (2010) 235–236, https://doi.org/10.3174/ajnr.A1987.
[15] R. Roskoski, Sunitinib: A VEGF and PDGF receptor protein kinase and angiogenesis inhibitor, Biochem. Biophys. Res. Commun. 356 (2) (2007) 323–328, https://doi.org/10.1016/j.bbrc.2007.02.156.
[16] T.A.T. Fong, L.K. Shawver, L. Sun, C. Tang, H. App, T.J. Powell, Y.H. Kim, R. Schreck, X. Wang, W. Risau, A. Ullrich, K.P. Hirth, G. McMahon, SU5416 is a potent and selective inhibitor of the vascular endothelial growth factor receptor (Flk-1/KDR) that inhibits tyrosine kinase catalysis, tumor vascularization, and growth of multiple tumor types, Cancer Res. 59 (1999) 99–106.
[17] S. Wilhelm, C. Carter, M. Lynch, T. Lowinger, J. Dumas, R.A. Smith, B. Schwartz, R. Simantov, S. Kelley, Discovery and development of sorafenib: A multikinase

inhibitor for treating cancer, Nat. Rev. Drug Discov. 5 (10) (2006) 835–844, https://doi.org/10.1038/nrd2130.
[18] G. Ranieri, G. Gadaleta-Caldarola, V. Goffredo, R. Patruno, A. Mangia, A. Rizzo, R. L. Sciorsci, C.D. Gadaleta, Sorafenib (BAY 43–9006) in Hepatocellular Carcinoma Patients: From Discovery to Clinical Development, Curr. Med. Chem. 19 (2012) 938–944, https://doi.org/10.2174/092986712799320736.
[19] Z. Han, Z. He, C. Wang, Q. Wang, The effect of apatinib in the treatment of sorafenib resistant metastatic hepatocellular carcinoma: A case report, Medicine (Baltimore). 97 (2018) 1–3, https://doi.org/10.1097/MD.0000000000013388.
[20] L. Huang, Z. Huang, Z. Bai, R. Xie, L. Sun, K. Lin, Development and strategies of VEGFR-2/KDR inhibitors, Futur. Sci. 4 (14) (2012) 1839–1852, https://doi.org/10.4155/fmc.12.121.
[21] C.M. Annunziata, A.J. Walker, L. Minasian, M. Yu, H. Kotz, B.J. Wood, K. Calvo, P. Choyke, D. Kimm, S.M. Steinberg, E.C. Kohn, Vandetanib, designed to inhibit VEGFR2 and EGFR signaling, had no clinical activity as monotherapy for recurrent ovarian cancer and no detectable modulation of VEGFR2, Clin. Cancer Res. 16 (2) (2010) 664–672, https://doi.org/10.1158/1078-0432.CCR-09-2308.
[22] A. Morabito, M.C. Piccirillo, F. Falasconi, G. De Feo, A. Del Giudice, J. Bryce, M. Di Maio, E. De Maio, N. Normanno, F. Perrone, Vandetanib (ZD6474), a dual inhibitor of vascular endothelial growth factor receptor (VEGFR) and epidermal growth factor receptor (EGFR) tyrosine kinases: current status and future directions, Oncologist. 14 (4) (2009) 378–390, https://doi.org/10.1634/theoncologist.2008-0261.
[23] H. Iwata, H. Oki, K. Okada, T. Takagi, M. Tawada, Y. Miyazaki, S. Imamura, A. Hori, J.D. Lawson, M.S. Hixon, H. Kimura, H. Miki, A back-to-front fragment-based drug design search strategy targeting the DFG-out pocket of protein tyrosine kinases, ACS Med. Chem. Lett. 3 (4) (2012) 342–346, https://doi.org/10.1021/ml3000403.
[24] M.E. Fraley, W.F. Hoffman, R.S. Rubino, R.W. Hungate, A.J. Tebben, R.Z. Rutledge, R.C. McFall, W.R. Huckle, R.L. Kendall, K.E. Coll, K.A. Thomas, Synthesis and initial SAR studies of 3,6-disubstituted pyrazolo[1,5-a]pyrimidines: A new class of KDR kinase inhibitors, Bioorg. Med. Chem. Lett. 12 (19) (2002) 2767–2770, https://doi.org/10.1016/S0960-894X(02)00525-5.
[25] M.E. Fraley, R.S. Rubino, W.F. Hoffman, S.R. Hambaugh, K.L. Arrington, R. W. Hungate, M.T. Bilodeau, A.J. Tebben, R.Z. Rutledge, R.L. Kendall, R.C. McFall, W.R. Huckle, K.E. Coll, K.A. Thomas, Optimization of a pyrazolo[1,5-a]pyrimidine class of KDR kinase inhibitors: Improvements in physical properties enhance cellular activity and pharmacokinetics, Bioorg. Med. Chem. Lett. 12 (24) (2002) 3537–3541, https://doi.org/10.1016/S0960-894X(02)00827-2.
[26] M.A. Aziz, R.A.T. Serya, D.S. Lasheen, A.K. Abdel-Aziz, A. Esmat, A.M. Mansour, A. N.B. Singab, K.A.M. Abouzid, Discovery of potent VEGFR-2 inhibitors based on furopyrimidine and thienopyrimidne scaffolds as cancer targeting agents, Sci. Rep. 6 (2016) 1–20, https://doi.org/10.1038/srep24460.
[27] Y. Liu, N.S. Gray, Rational design of inhibitors that bind to inactive kinase conformations, Nat. Chem. Biol. 2 (7) (2006) 358–364, https://doi.org/10.1038/nchembio799.
[28] J. Blanc, R. Geney, C. Menet, Type II Kinase Inhibitors: An Opportunity in Cancer for Rational Design, Anticancer Agents Med. Chem. 13 (2013) 731–747, https://doi.org/10.2174/1871520611313050008.
[29] S.J. Modi, V.M. Kulkarni, Vascular endothelial growth factor receptor (VEGFR-2)/KDR inhibitors: Medicinal chemistry perspective, Med. Drug Discov. 2 (2019) 1–25, https://doi.org/10.1016/j.medidd.2019.100009.
[30] J. Han, S.J. Kaspersen, S. Nervik, K.G. Nørsett, E. Sundby, B.H. Hoff, Chiral 6-aryl-furo[2,3-d]pyrimidin-4-amines as EGFR inhibitors, Eur. J. Med. Chem. 119 (2016) 278–299, https://doi.org/10.1016/j.ejmech.2016.04.054.
[31] J. Sun, M.-Y. Yang, C.-G. Yan, One–pot reaction for the convenient synthesis of functionalized 2-oxaspiro[bicyclo[2.2.1]heptane-2,3′-indolines], Chem. Sel. 2 (1) (2017) 304–308, https://doi.org/10.1002/slct.201600929.
[32] A. De Nino, L. Maiuolo, M. Nardi, R. Pasceri, A. Procopio, B. Russo, Development of one-pot three component reaction for the synthesis of N'-aryl-N-cyanoformamidines, essential precursors of formamidine pesticides family, Arab. J. Chem. 9 (1) (2016) 32–37, https://doi.org/10.1016/j.arabjc.2015.06.016.
[33] M. Soleimany, J. Lari, H. Vahedi, M. Imanpour, New facile route to synthesize furo [3,2-e][1,2,4]triazolo[4,3-c]pyrimidine and furo[3,2-e][1,2,4]triazolo[1,5-c] pyrimidine derivatives, Synth. Commun. 44 (23) (2014) 3375–3383, https://doi.org/10.1080/00397911.2014.943344.
[34] H. Sunil, R. Vikas, P. Pravin, H. Priyanka, N. Sampat, A. Sandip, S. Anand, Synthesis, characterization and anti-microbial evaluation of some 2- iodo-N'-[(1E)-substituted phenylmethylidene] benzohydrazide analogues, Int. J. Pharm. Sci. Drug Res. 2 (2010) 134–136.
[35] P. Majumdar, A. Pati, M. Patra, R.K. Behera, A.K. Behera, Acid hydrazides, potent reagents for synthesis of oxygen-, nitrogen-, and/or sulfur-containing heterocyclic rings, Chem. Rev. 114 (5) (2014) 2942–2977, https://doi.org/10.1021/cr300122t.
[36] H.H. Fox, J.T. Gibas, Synthetic tuberculostats. IV. pyridine carboxylic acid hydrazides and benzoic acid hydrazides, J. Org. Chem. 17 (12) (1952) 1653–1660, https://doi.org/10.1021/jo50012a013.
[37] M. Sato, R. Ohta, Liquid crystalline semirigid polyesters based on phenylstilbene analogues of 1,3,4-thiadiazole, Liq. Cryst. 34 (3) (2007) 295–303, https://doi.org/10.1080/02678290600858066.
[38] A.T. Ali, M.H. Hekal, Convenient synthesis and anti-proliferative activity of some benzochromenes and chromenotriazolopyrimidines under classical methods and phase transfer catalysis, Synth. Commun. 49 (24) (2019) 3498–3509, https://doi.org/10.1080/00397911.2019.1675173.
[39] R.M. Shaker, Synthesis of new furo[2,3-d]pyrimidines and furo[3,2-e][1,2,4] triazolo[1,5-c]pyrimidines, ARKIVOC. 14 (2006) 68–77.
[40] H.M. Hassaneen, W.W. Wardakhan, Y.S. Mohammed, Synthesis and reactions of pyrido[2,1-a]isoquinolin-4-yl formimidate derivatives and antimicrobial activities of isolated products, J. Heterocycl. Chem. 54 (5) (2017) 2850–2858, https://doi.org/10.1002/jhet.v54.510.1002/jhet.2891.
[41] Y. Xin, J. Yuan, Schiff's base as a stimuli-responsive linker in polymer chemistry, Polym. Chem. 3 (2012) 3045–3055, https://doi.org/10.1039/c2py20290e.
[42] P.G. Mandhane, R.S. Joshi, D.R. Nagargoje, A.V. Chate, C.H. Gill, Ultrasonic promoted synthesis and antibacterial screening of some novel piperidine incorporated α-aminophosphonates, Phosphorus, Sulfur Silicon Relat. Elem. 186 (1) (2011) 149–158, https://doi.org/10.1080/10426507.2010.492363.
[43] R.S. Joshi, P.G. Mandhane, S.D. Diwakar, S.K. Dabhade, C.H. Gill, Synthesis, analgesic and anti-inflammatory activities of some novel pyrazolines derivatives, Bioorg. Med. Chem. Lett. 20 (12) (2010) 3721–3725, https://doi.org/10.1016/j.bmcl.2010.04.082.
[44] M. Mečiarová, Š. Toma, P. Magdolen, Ultrasound effect on the aromatic nucleophilic substitution reactions on some haloarenes, Ultrason. Sonochem. 10 (4-5) (2003) 265–270, https://doi.org/10.1016/S1350-4177(02)00157-8.
[45] Z.Q. Liang, C.X. Wang, J.X. Yang, H.W. Gao, Y.P. Tian, X.T. Tao, M.H. Jiang, A highly selective colorimetric chemosensor for detecting the respective amounts of iron(II) and iron(III) ions in water, New J. Chem. 31 (2007) 906–910, https://doi.org/10.1039/b701201m.
[46] Z.A. Hozien, A.F.M. EL-Mahdy, A. Abo Markeb, L.S.A. Ali, H.A.H. El-Sherief, Synthesis of Schiff and Mannich bases of new s-triazole derivatives and their potential applications for removal of heavy metals from aqueous solution and as antimicrobial agents, RCS Adv. 10 (34) (2020) 20184–20194, https://doi.org/10.1039/D0RA02872J.
[47] A. Al-kadhimi, N. Al-azzawi, A. Khalaf, Facile synthesis of Schiff and Mannich bases of isatin derivatives, J. Chem. Biol. Phys. Sci. 5 (2015) 2338.
[48] M. Tugrak, H.I. Gul, H. Sakagami, E. Mete, Synthesis and anticancer properties of mono Mannich bases containing vanillin moiety, Med. Chem. Res. 26 (7) (2017) 1528–1534, https://doi.org/10.1007/s00044-017-1833-x.
[49] A.E.M. Noreljaleel, H.M.A. Fadul, J.H. Van Der Westhuizen, M.A. Karim, S.M. H. Ayuob, M.J.A. Abualreish, Synthesis and structural elucidation of 4-hydroxy-3-methoxy-5- aminomethylbenzaldehydes, Asian J. Org. Med. Chem. 3 (2018) 50–53. https://doi.org/10.14233/ajomc.2018.ajomc-p124.
[50] M.D. Shultz, Setting expectations in molecular optimizations: Strengths and limitations of commonly used composite parameters, Bioorg. Med. Chem. Lett. 23 (21) (2013) 5980–5991, https://doi.org/10.1016/j.bmcl.2013.08.029.
[51] S. Jie, H. Li, Y. Tian, D. Guo, J. Zhu, S. Gao, L. Jiang, Berberine inhibits angiogenic potential of Hep G2 cell line through VEGF down-regulation in vitro, J. Gastroenterol. Hepatol. 26 (2011) 179–185, https://doi.org/10.1111/j.1440-1746.2010.06389.x.
[52] R.P. Singh, S. Dhanalakshmi, C. Agarwal, R. Agarwal, Silibinin strongly inhibits growth and survival of human endothelial cells via cell cycle arrest and downregulation of surviving, Akt and NF-κB: implications for angioprevention and antiangiogenic therapy, Oncogene 24 (2005) 1188–1202, https://doi.org/10.1038/sj.onc.1208276.
[53] K.M. Malinda, A.L. Goldstein, H.K. Kueinman, Thymosin β4 stimulates directional migration of human umbilical vein endothelial cells, FASEB J. 11 (6) (1997) 474–481, https://doi.org/10.1096/fsb2.v11.610.1096/fasebj.11.6.9194528.
[54] J. Pijuan, C. Barceló, D.F. Moreno, O. Maiques, P. Sisó, R.M. Marti, A. Macià, A. Panosa, In vitro cell migration, invasion, and adhesion assays: From cell imaging to data analysis, Front. Cell Dev. Biol. 7 (2019) 1–16, https://doi.org/10.3389/fcell.2019.00107.
[55] D.A. Lauffenburger, A.F. Horwitz, Cell migration: A physically integrated molecular process, Cell 84 (1996) 359–369.
[56] R. Horwitz, D. Webb, Cell migration, Curr. Biol. 13 (19) (2003) R756–R759.
[57] A.J. Ridley, M.A. Schwartz, K. Burridge, R.A. Firtel, M.H. Ginsberg, G. Borisy, J. T. Parsons, A.R. Horwitz, Cell Migration: Integrating Signals from Front to Back, Sci. 302 (2003) 1704–1709, https://doi.org/10.1126/science.1092053.
[58] M. McTigue, B.W. Murray, J.H. Chen, Y.-L. Deng, J. Solowiej, R.S. Kania, Molecular conformations, interactions, and properties associated with drug efficiency and clinical performance among VEGFR TK inhibitors, Proc. Natl. Acad. Sci. U. S. A. 109 (45) (2012) 18281–18289, https://doi.org/10.1073/pnas.1207759109.
[59] K. Okamoto, M. Ikemori-Kawada, A. Jestel, K. von König, Y. Funahashi, T. Matsushima, A. Tsuruoka, A. Inoue, J. Matsui, Distinct binding mode of multikinase inhibitor lenvatinib revealed by biochemical characterization, ACS Med. Chem. Lett. 6 (1) (2015) 89–94, https://doi.org/10.1021/ml500394m.
[60] A. Daina, O. Michielin, V. Zoete, SwissADME: A free web tool to evaluate pharmacokinetics, drug-likeness and medicinal chemistry friendliness of small molecules, Sci. Rep. 7 (2017) 1–13, https://doi.org/10.1038/srep42717.
[61] C. Tang, C. Li, S. Zhang, Z. Hu, J. Wu, C. Dong, J. Huang, H.-B. Zhou, Novel bioactive hybrid compound dual targeting estrogen receptor and histone deacetylase for the treatment of breast cancer, J. Med. Chem. 58 (11) (2015) 4550–4572, https://doi.org/10.1021/acs.jmedchem.5b00099.
[62] M.V. Adhikari, S.D. Samant, Sonochemical bromination of acetophenones using p-toluenesulfonic acid-N-bromosuccinimide, Ultrason. Sonochem. 9 (2) (2002) 107–111, https://doi.org/10.1016/S1350-4177(01)00108-0.
[63] C. Li, C. Tang, Z. Hu, C. Zhao, C. Li, S. Zhang, C. Dong, H.-B. Zhou, J. Huang, Synthesis and structure-activity relationships of novel hybrid ferrocenyl compounds based on a bicyclic core skeleton for breast cancer therapy, Bioorg.

Med. Chem. 24 (13) (2016) 3062–3074, https://doi.org/10.1016/j.bmc.2016.05.019.
[64] C. Fontanella, E. Ongaro, S. Bolzonello, M. Guardascione, G. Fasola, G. Aprile, Clinical advances in the development of novel VEGFR2 inhibitors, Ann. Transl. Med. 2 (2014) 1–10, https://doi.org/10.3978/j.issn.2305-5839.2014.08.14.
[65] K. Sharma, P.S. Suresh, R. Mullangi, N.R. Srinivas, Quantitation of VEGFR2 (vascular endothelial growth factor receptor) inhibitors - review of assay methodologies and perspectives, Biomed. Chromatogr. 29 (6) (2015) 803–834, https://doi.org/10.1002/bmc.v29.610.1002/bmc.3370.
[66] T. Mosmann, Rapid colorimetric assay for cellular growth and survival: application to proliferation and cytotoxicity assays, J. Immunol. Methods. 65 (1983) 55–63, https://doi.org/10.1039/c6ra17788c.
[67] D. Tao, J. Wu, Y. Feng, J. Qin, J. Hu, J. Gong, New method for the analysis of cell cycle-specific apoptosis, Cytom. Part A 57A (2) (2004) 70–74, https://doi.org/10.1002/(ISSN)1097-032010.1002/cyto.a.v57a:210.1002/cyto.a.10117.